

Università degli Studi di Genova
Scuola Politecnica
DICAT

Swiss Federal Institute of Technology Zurich
Department of Mechanical and Process Engineering
Institute of Fluid Dynamics



Numerical Prediction of the Pressure in the Vicinity of an Intra-Cochlear Receiver

Author: Alberto Spirito

Supervisors: Prof. Alessandro Bottaro
Prof. Dominik Obrist

October 2013

Abstract

This work aims to give instructions for future developments of cochlear implants. In the last years, the procedures and the devices involved in these implants have been widely studied to present new configurations which intend to solve the problems of the first arrangements proposed. The increasing market and importance of this kind of implants gives impulse for further investigations on this matter. This work intends to study the feasibility of a new arrangement proposed for cochlear implants, using a numerical model to simulate the interested parts. This work is structured in four parts. In the first part a literature review is made; it is necessary to present and understand the main points of this thesis. After this introductory part, the method and the hypotheses which are used to simulate the elements object of this study are outlined. In the third part the results obtained are presented, explaining the consequences and the considerations which arise from them. A final chapter summarizes the conclusions resulting from this work, and presents some ideas for future works on this topic.

Prefazione

Questo lavoro concerne la simulazione numerica della coclea. La coclea è un organo dell'orecchio, che ha la funzione di trasformare il segnale vibro-acustico proveniente dalla catena di ossicini attaccata al timpano, in un segnale elettrico che viene poi processato dal cervello. La coclea è un elemento fondamentale nella catena degli organi che permette la percezione del suono.

La simulazione numerica della coclea è fondamentale per la scoperta di meccanismi che governano la sua dinamica. Ad oggi, molti processi fisici della coclea non sono ancora completamente compresi. D'altra parte, però, il crescente mercato di apparecchi uditivi di vario genere richiede una profonda conoscenza dei processi cocleari. Per questo motivo, i differenti fenomeni coinvolti nella meccanica dell'orecchio interno devono essere risolti e descritti da appropriati modelli fisici.

Tra i vari dispositivi dei quali è studiato lo sviluppo c'è l'impianto cocleare. L'impianto cocleare è un orecchio artificiale che aiuta persone sorde, o con udito estremamente danneggiato, ad acquistare una percezione uditiva. Tradizionalmente questi tipi di impianti sono stati applicati in due parti distinte: una interna ed una esterna. A causa di questa configurazione, e specialmente a causa dell'esistenza di una parte esterna, l'utilizzo di questo tipo di impianti ha alcune limitazioni, per esempio: devono essere spenti quando immersi in acqua, sono spesso origine di infezioni e sono molto sensibili a variazioni di pressione. Senza considerare che l'appendice esterna è anche la parte più scomoda per gli utilizzatori di questo tipo di apparecchiature. Per questo motivo è stata proposta una configurazione

Prefazione

per l'impianto cocleare che include tutte le sue parti sotto l'osso temporale, ovvero una struttura senza appendici esterne. Questo tipo di configurazione è resa possibile grazie alla messa a punto del ricevitore intra-cocleare, la cui implementazione nella coclea è studiata nel corso di questa tesi.

L'obiettivo di questo progetto è approssimare lo studio numerico della integrazione di un modello del ricevitore intra-cocleare all'interno della coclea. Per perseguire questo obiettivo, è stato prima necessario cambiare la configurazione del box cocleare tradizionalmente utilizzato per la simulazione della coclea, questo perché il modello tradizionale non permette una adeguata riproduzione del flusso nella regione in cui verrà collocato il microfono (che rappresenta la parte del ricevitore intra-cocleare che è implementata nella coclea). Successivamente, è stato introdotto il modello del microfono all'interno del box e sono stati studiati i suoi effetti sulla dinamica della coclea.

Questo lavoro è stato strutturato in quattro parti. Nella prima parte si introducono i concetti fondamentali, necessari per capire i principali problemi e processi fisici che interessano questa tesi. Nella seconda parte è spiegato approfonditamente il metodo utilizzato per simulare la coclea e le diverse configurazioni testate. Nella terza parte sono presentati i risultati ottenuti nel corso di questo lavoro. Visto che il lavoro si può suddividere in due fasi, ovvero una fase riguardante lo studio di una nuova configurazione per il box cocleare e l'altra concernente l'introduzione del microfono, anche il capitolo dei risultati è diviso in due parti per trattare separatamente ciascuna delle due fasi del lavoro. Infine, nella ultima parte sono raccolte tutte le conclusioni desunte dallo studio svolto e consigli per eventuali sviluppi di questo lavoro.

Chapter 1

Introduction

This thesis deals with the numerical simulation of the motion of fluid in the cochlea. The cochlea is an organ of the ear, whose function is to transform the pressure wave of a sound signal into an electrical signal which is sent to the brain. It is a core element in the chain of organs that allows the perception of hearing.

Cochlea modelling is an important issue and many aspects of cochlear dynamics are not yet fully understood. On the other hand, the increasing market of hearing aids of various kinds requires close insight on cochlear processes. Therefore, the different phenomena involved in the mechanics of the inner ear have to be resolved and described by appropriate physical models.

Among the devices whose development is studied there is the cochlear implant. The cochlear implant is an artificial ear that helps deaf or severely hearing impaired people to gain a sense of sound. Traditionally, this device has been implemented divided into two parts: one external and one internal. As a result, especially for the presence of the external parts, the use of such implants has some limitations, for example: they have to be switched off when swimming, they are the most frequent origin of infections and they are sensitive to pressure variations. Furthermore the external appendix is the most uncomfortable part for the patients. For this reason a cochlear

implant has been proposed which contains all of its parts underneath the temporal bone, i.e. a completely internal cochlear implant. This new layout is made possible by the intracochlear receiver whose feasibility is now under study.

The goal of this project is to approach the numerical study of the integration in the cochlea of the intracochlear receiver. To achieve this objective, it was first necessary to change the configuration of the cochlear box used to simulate numerically the behaviour of the cochlea, because the traditional cochlear box does not reproduce adequately the fluid flow in the region in which the microphone (i.e. the part of the intracochlear receiver which is implemented inside the cochlea) will be inserted. Subsequently, a model of the microphone has been inserted and its effects on cochlear dynamics have been assessed.

This thesis has been structured in four parts. In the first a literature review explains the concepts necessary to understand the main points of the work. The second part the method utilized to simulate the cochlea and the different configurations tested is described. In the third part the results obtained are presented, and, as the work has been divided in two steps (i.e. the change of the cochlear box and the subsequent implementation of the microphone model), also this chapter deals separately with each topic. Finally, the conclusions of this work and the possible developments proposed for future studies are presented.

Chapter 2

Literature review

Although the focus of this thesis is on cochlea modelling, a quick overview of the main organs participating in the hearing process is necessary to have a better insight into the main physical problems involved in this work. After an explanation of the hearing flow, the cochlear implants are introduced, a different configuration of which is analyzed in this thesis. Finally the immersed boundary method, which has been used in this study to implement all the surfaces immersed in the cochlea, is presented.

2.1 Hearing process

The human ear can detect frequencies in the range between 20 Hz and 20 kHz, the highest sensitivity is located between 2 and 4 kHz [2]. The hearing process is structured in different stages. Sound waves reaching the ear are first collected and converted in electrical signals in the auditory system. These signals are then transmitted to the brain via the auditory nerve: finally inside the brain the message is decoded to yield the perception of the sound.

2.1. Hearing process

2.1.1 The auditory system

The ear comprises the auditory system and consists of three parts: the outer ear, the middle ear and the inner ear (fig. 2.1).

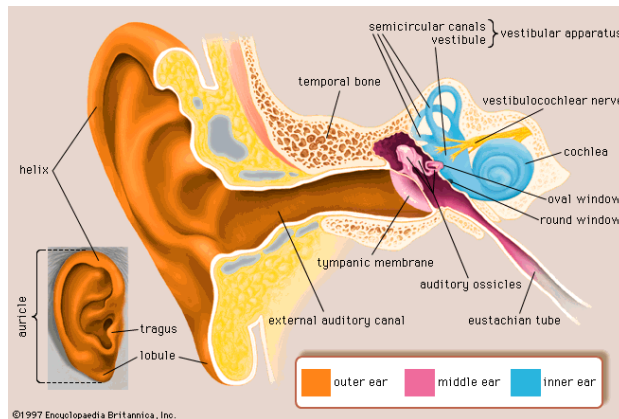


Figure 2.1: Anatomy of human ear [4].

- In the *outer ear* the sound signal is gathered and transmitted through the ear canal with an additional information to establish the source location. Several cartilaginous folds, called *pinna*, surround the ear: when the sound wave hits the pinna it is reflected and attenuated, so that the sound signal is provided with an information which will be used by the brain to determine the direction from which the sound comes.
- The *middle ear* works as an amplifier of sound pressure signal. At the end of the ear canal stands the *tympanic membrane* (eardrum), attached to the other side of the eardrum there is a chain of delicate bones, which are, in order following the path of the wave: *malleus* (hammer), *incus* (anvil), and *stapes* (stirrup). When the sound wave reaches the tympanic membrane, these ossicles act as a lever, converting the lower-pressure sound vibrations at the tympanic membrane

into higher-pressure sound vibrations at another, smaller membrane called the *oval* (or elliptical) *window*. The gain of the ossicular chain changes with the pressure signal frequency.

- In the *inner ear* the sound wave is finally converted to an electrical signal. The organ that allows this task is the *cochlea*, that receives the signal from the stapes via the oval window and acts the transformation with a complex process. In addition to the hearing sense, the inner ear also hosts the primary sensors of our balance sense, that are not interesting for the purposes of this work.

Fig. 2.2 summarizes the process described.

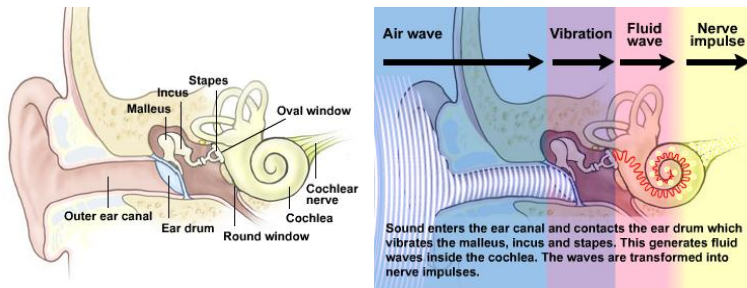


Figure 2.2: Anatomy (left) and physiology (right) of human ear [14].

2.1.2 Anatomy of the cochlea

The present work addresses only the inner ear, and specifically the modelling of the cochlea. It is important to underline the main features of this organ.

The cochlea is a hollow-coiled structure that is placed in the human temporal bone. The human cochlea has 2.5 turns and an uncoiled length of about 35 mm [1]. The physiological function of the coiling of the cochlea is not fully understood, recently it was suggested that the coiling produces an amplification of the low-frequency signals, supporting the hearing at low

2.1. Hearing process

frequencies [23]. Fig. 2.3 illustrates a simplified sketch of the coiled cochlea structure.

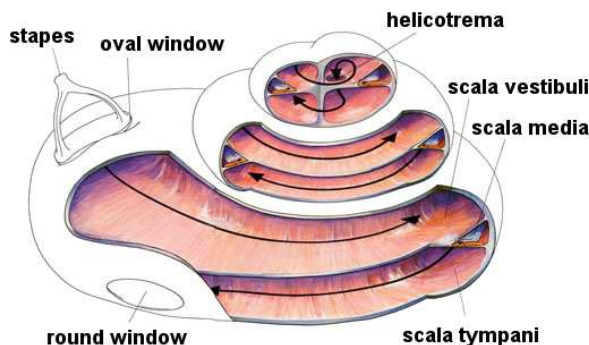


Figure 2.3: Coiled human cochlea [2].

The cross section of the cochlea, shown in fig. 2.4, is divided in three canals: the *scala tympani*, the *scala vestibuli* and the *scala media*. All of them are fluid-filled. Specifically the *scala vestibuli* and the *scala tympani* contains a liquid called *perilymph* whereas the *scala media* contains *endolymph*. Between the two fluids there are differences in ion content, these different compositions are essential to generate electrical nerve signals. Two membranes separates the three ducts: the *Reissner's membrane* lies between *scala vestibuli* and *scala media* while the *basilar membrane* is located between *scala tympani* and *scala media*. Furthermore, at the far end of the cochlea (*apex* or apical end), there is an opening, named *helicotrema*, which connects the *scala vestibuli* and *scala tympani*. At the beginning of the cochlea (*base* or basal end), there are two membrane-covered openings: one in the *scala vestibuli*, called the *oval window*, and one in *scala tympani*, the *round window*, see fig. 2.3. The membranes that cover these two holes are relatively soft and they allow the fluid inside the cochlea to move.

Within the *scala media*, on the *basilar membrane* and along its entire length, lies the organ of Corti (see fig. 2.4 and fig. 2.5). This is a complex fluid-filled system, whose internal mechanisms and processes are not yet

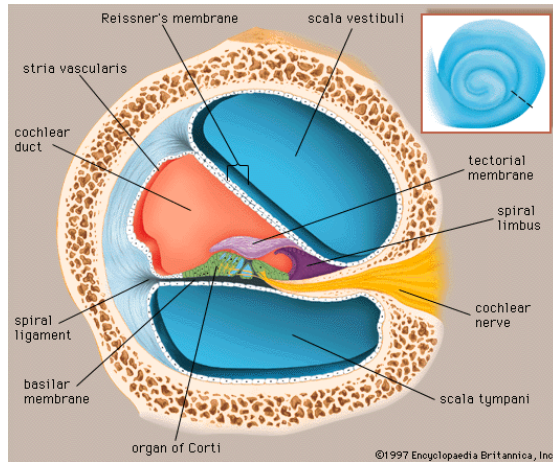


Figure 2.4: Cross section of the cochlea [4].

fully understood. It includes several membranes, structural elements, fluid spaces and two types of *hair cells*: *inner* hair cells and *outer* hair cells. The hair cells are columnar cells, with several *stereocilia* on top of them (around 60 on inner hair cells, 100 to 120 on outer hair cells [10]). The stereociliae are the mechanoreceptors for hearing sense. Along the organ of Corti there are three rows of outer hair cells and one row of inner hair cells; the former are directly connected to the *tectorial membrane* (a membrane that partially covers the organ of Corti, see fig. 2.5) through some stereocilia, while the latter are not in contact with the membrane. In resting position there is a potential difference across the outer membrane of the hair cells. 95% of the nerve fibres, which depart from the hair cell, are afferent fibres and lead the electrical signal from the inner hair cells to the brain. The remaining part is composed of efferent fibres and are almost entirely connected to the outer hair cells.

2.1. Hearing process

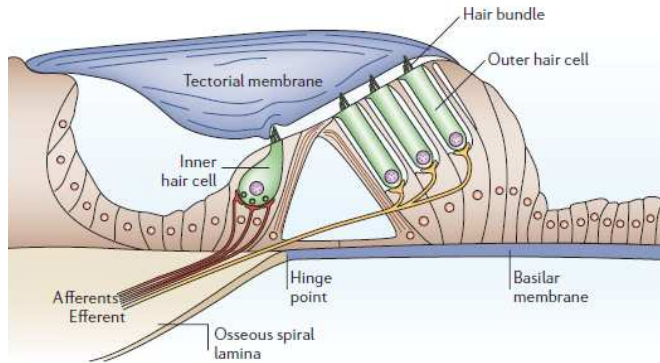


Figure 2.5: Organ of Corti [2].

2.1.3 Physiology of the Cochlea

As previously explained, the stapes is attached to the oval window. When a sound wave reaches the tympanic membrane, the chain of ossicles in the middle ear moves, as a consequence the stapes pushes the oval window. The stimulation of the oval window, in turn, induces a travelling wave within the fluid of the cochlea; furthermore it provokes the movement of the *cochlear partition*. Cochlear partition is the name commonly used to refer to the flexible structure that separates the scala tympani from the scala vestibuli. As a result, it includes all the structures contained in the scala media and its bounding membranes (i.e. basilar and Reissner's membrane). Fig. 2.6 shows a schematic of the process triggered by stapes movement.

Within the cochlea, the sound signal is decomposed into its underlying frequencies. This process is achieved through the specific anatomy of the basilar membrane. The stiffness of the basilar membrane decreases by several orders of magnitude passing from the base to the apex; as a consequence, each location of its extent is tuned to a particular frequency. If the oval window oscillates at a specific frequency, a travelling wave is generated on the basilar membrane. Due to basilar membrane's structure just one

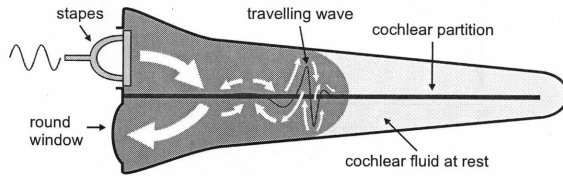


Figure 2.6: Schematic of a travelling wave provoked by a sinusoidal oscillation of the stapes [3].

point reaches the maximum displacement, the one that is in resonance at this particular frequency. This point is specific for the frequency of the signal, it is therefore called *characteristic place* (or *characteristic point*) of that frequency. Behind the characteristic point the displacement amplitude falls to zero quickly. High frequencies are encoded towards the apex of the membrane while low frequencies have their characteristic place towards the base. This feature is shown in fig. 2.7.

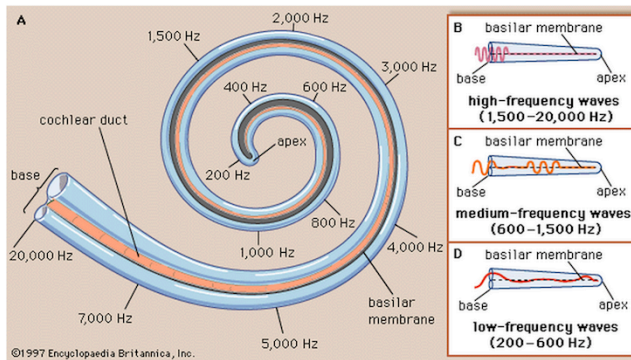


Figure 2.7: Tonotopic map of frequency decomposition [4].

When the basilar membrane is deflected, the organ of Corti follows its movement, and consequently the hair cells are deflected. As a result positive ions from the endolymph enter the hair cells, depolarizing them.

2.2. Cochlear implant

The depolarization results in a variation of the potential between the hair cells and the fluid, thus it generates an electrical signal that is sent to the brain through the nerve cells. As explained in the previous section, the outer hair cells are directly connected to the tectorial membrane, as a result they are mechanically deflected by the shearing motion of the membrane. On the contrary, the inner hair cells, move due to the motion of the endolymphatic fluid within the scala media.

As the inner hair cells are connected to the afferent nerve cells, they are responsible for the signal sent to the central nervous system. On the other hand, the outer hair cells are controlled by the central nervous system, and this disposition allows the process of *active amplification*. Although it is widely accepted that the effects of active processes are essential on cochlear output signal (see for example [10]), they are not implemented in the model of the cochlea used for this study. The response of a "dead" cochlea (i.e. a cochlea extracted from a cadaver) is not affected by active processes as they are possible only in cochleas of living human being.

2.2 Cochlear implant

The cochlear implant is an artificial ear that helps deaf or hearing impaired people to gain a sense of sound.

Cochlear implants are surgically implemented in people who are not able to hear because of damage to sensory hair cells in their cochlea. When applied to the patients, they provide sufficient hearing. Although the sound informations received by the brain are less compared to those provided by a properly working cochlea, the patients can effectively hear speech and environmental sounds [14].

In simple terms, this implant works receiving the sound from the environment through a microphone, subsequently a chain of components (see below) processes the signal and selectively send it to the electrodes placed in the cochlea. These electrodes stimulate directly the nerve cells, by-passing all the physical processes that in a working ear are carried out by the auditory system.

In the last years cochlear implants have been developed considerably, a basic configuration will be presented. The main components of a cochlear implant are showed in fig. 2.8.

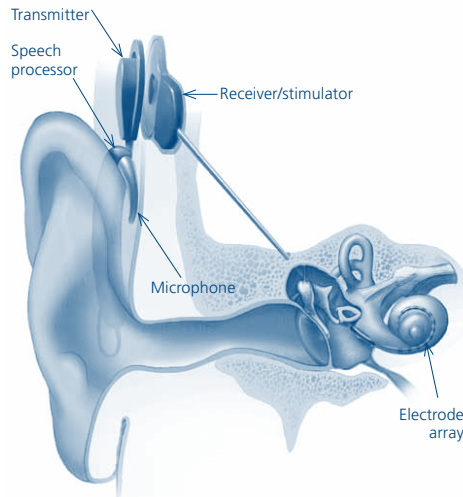


Figure 2.8: Ear with a cochlear implant [19].

Cochlear implants can be divided into two parts: the external part and the internal part. The external part includes:

- one (or more) *microphone* which detects the sound coming from the environment;
- the *speech processor*, which acts as a filter, prioritizing the frequencies of the audible speech. This task commonly uses a Fast Fourier Transforms (FFT), which divides the signal into frequency bands. The algorithm chooses a number of the strongest outputs from the filters, this number depends on internal part characteristics. The signal, split among different channels, is sent through a thin cable to the transmitter;
- the *transmitter* is basically a coil which works sending the sound signal

2.2. Cochlear implant

by electromagnetic induction. It is held in position by a little magnet placed behind the external ear (fig. 2.8). This component transmits the signal to the internal portion of the device over a radio frequency link: in this way there is no need for a physical connection that would increase the chances of infections and pain.

Fig. 2.9 illustrates a detailed picture of the internal component of the cochlear implant, which is usually referred to as *intracochlear receiver*.



Figure 2.9: Intracochlear receiver [14].

The intracochlear receiver includes two parts:

- the *receiver*, that receives the electromagnetic signal from the transmitter, and sends it to the electrodes placed in the cochlea. This device also receives from the transmitter the power that it needs to work. Furthermore it works as a computer, translating the information coming from the transmitter, and controlling the electrical current sent to the electrodes. It is placed on the skull, behind the ear;

- the *electrode array* is an array that can have 22 or more electrodes [19] placed in the cochlea. The electrode array is made from a type of silicone rubber, while the electrodes are made of platinum or a similar highly conductive material. The high conductivity of the electrodes is necessary to transmit the signal to the afferent nerve cells in the organ of Corti. When an electrical current is routed to an intracochlear electrode, an electrical field is generated and auditory nerve fibers are stimulated. The electrode array does not reach the apex of the cochlea due to physical limitations, usually it covers around 25 millimeters of the cochlea (cochlea length is around 36 millimeters, see 2.1.2), which means that the upper limit of hearing with this device is decreased to about 6 kHz. This component increases also the lower limit of hearing to a value of about 400 Hz.

2.3 Immersed boundary method

The Immersed Boundary Method (IBM) was first implemented by Peskin [7], who used it to simulate the interaction between the flexible heart valves and the blood flow. Since then, it was developed and used for a wide variety of problems in which an analysis of fluid flow interacting with flexible structures with complex geometries was needed.

The IBM is implemented using two grids: an Eulerian grid, used to solve the fluid flow, and a Lagrangian grid that follows the points of the flexible structure. There is no need for a specific relation between the Eulerian and Lagrangian grid; the interactions between fluid and the immersed boundary are implemented through a discrete function, that overcomes the non-correspondence between Eulerian and Lagrangian points. The IBM operates implementing the effects of the coupling between the two grids separately on each subsystem; therefore the fluid side feels the presence of the immersed boundary through a set of forces that arise because the membrane has been displaced and deformed with respect of its original shape. On the other hand, the solid structure is forced to have the same local velocity of the fluid, because it is in contact with the surrounding fluid and

2.3. Immersed boundary method

thus the velocity has to be consistent with the no-slip boundary condition.

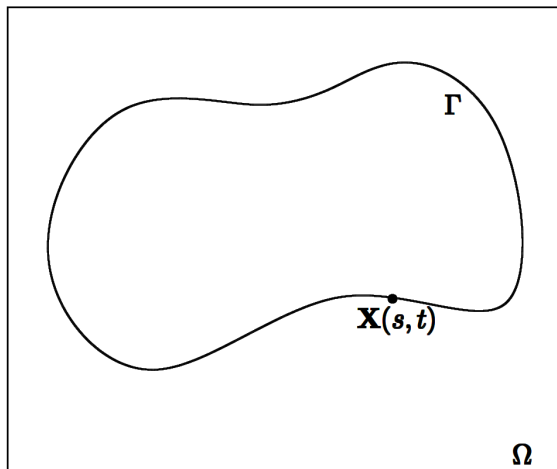


Figure 2.10: Example of immersed boundary curve (Γ), in a fluid domain (Ω) and described by the function $\mathbf{X}(s, t)$.

Fig. 2.10 shows an example of a generic immersed boundary in a fluid domain. The IBM can be applied to solve the fluid dynamic equations in the fluid, with the following set of equations [8]

$$\mathbf{F}(s, t) = A_f \mathbf{X}(s, t), \quad (2.1)$$

$$\mathbf{f}(\mathbf{x}, t) = \int_{\Gamma} \mathbf{F}(s, t) \delta(\mathbf{x} - \mathbf{X}(s, t)) ds, \quad (2.2)$$

$$\begin{cases} \frac{\partial \mathbf{u}}{\partial t} + \mathbf{u} \cdot \nabla \mathbf{u} = -\nabla p + \frac{1}{Re} \nabla^2 \mathbf{u} + \mathbf{f}, \\ \nabla \cdot \mathbf{u} = 0 \end{cases}, \quad (2.3)$$

$$\frac{\partial \mathbf{X}(s, t)}{\partial t} = \mathbf{u}(\mathbf{X}(s, t), t) = \int_{\Omega} \mathbf{u}(\mathbf{x}, t) \delta(\mathbf{x} - \mathbf{X}(s, t)) dx, \quad (2.4)$$

lower-case variables are used for Eulerian quantities and upper-case letters for the Lagrangian ones; $\mathbf{X}(s, t)$ is the vector function giving the location of

points of the immersed boundary in the domain as a function of arclength s and time t ; \mathbf{f} is the forcing term which serves to model the effects of the boundary; \mathbf{F} is the force applied by the boundary to the fluid. A_f is the force generation operator and it depends on the structure and properties of the membrane.

These equations shows the basic steps of the IBM just described. Equation (2.1) calculates the force that the immersed boundary applies due to its current configurations. Equation (2.2) spreads said force, defined on the Lagrangian point, to the nearby Eulerian point. To perceive this, a defined discrete delta function δ , that has to satisfy some properties, is utilized. Equation (2.3) are the Navier-Stokes and continuity equations that solve the flow to which the forcing term \mathbf{f} just obtained is applied. Equation (2.4) interpolate the velocity from the Eulerian field to the Lagrangian one in order to provide a velocity vector on each point of the membrane.

Chapter 3

Method

The flow solver used to run the simulations for this work is called "IMPACT", it was developed by Henniger [6]. Edom adapted this code to simulate the flow in the cochlea [5] and I implemented my modifications on her model.

The numerical modelling of the cochlea is a complex issue. Until now, nobody developed a numerical method that can take into account all the phenomena involved in cochlear dynamics. This chapter goes through the specific numerical model used in this work to simulate the dynamic of the cochlea, explaining its main features.

3.1 Computational model of the cochlea

3.1.1 Hypotheses of the model

The specifications implemented in the model of this thesis are the following:

- *two-dimensional box* for simulation of cochlea geometry, the coiled structure of the cochlea has been ideally stretched out on a plane, fig. 3.1 shows one example of two-dimensional box used for some simulations in this work;

3.1. Computational model of the cochlea

- *passive mode*, active amplification (see end of sec. 2.1.3) is neglected in this model;
- *incompressible flow*, furthermore the fluid is supposed to *behave like water* (i.e. same viscosity and density);
- *no modelling of cochlear partition structures except for the basilar membrane*, this means that the model considered is a *two-chamber model*, scala vestibuli and scala tympani are the chambers considered in the simulation;
- *immersed boundary method* for the implementation of basilar membrane forces on the fluid;
- *intramembrane forces* on basilar membrane are considered on both direction, with *stiffnesses exponentially decreasing* along cochlear length, and *zero mass and damping* forces;
- *zero round window stiffness*.

3.1.2 Insight into the hypotheses

The two dimensional box is the set up most frequently utilized in the scientific world for simulations of the cochlea. It provides sufficient insight into the main features of the cochlea with a shorter simulation time and a relatively lower complexity of the code. Some 3D models were implemented (see for example [9]): considering the properties that are inspected in this work, a two-dimensional model (one example of it is depicted in fig. 3.1) is considered adequate.

Active amplification has a great effect on cochlear output signal [11], and this model does not include it. The implementation of active processes in the code of this thesis is proposed as a future work for further investigations on cochlea dynamics.

From a mechanical point of view, perilymph has the same properties of water. The incompressibility assumption is considered valid as the acoustic

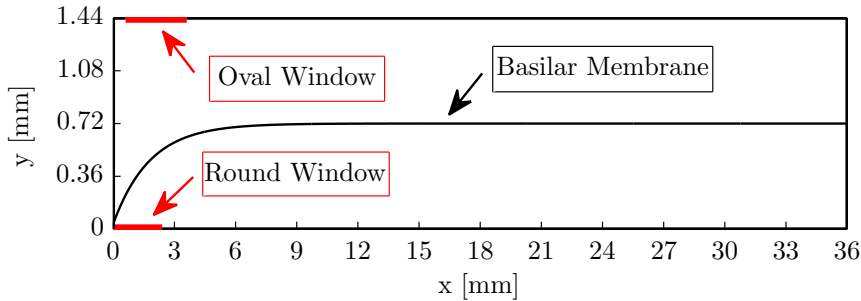


Figure 3.1: 2-D box for cochlear simulation

wave length is much larger than the length of the cochlea in the range of the relevant physiological frequencies.

It has been stated that "the crux in cochlear mechanics is the large range of scales and physical phenomena which operate simultaneously and interactively" [2]. There is a tight interaction between the different components of the cochlea as shown in fig. 3.2. The implementation of all these processes would be a complex task, a complete model should include several scales and different modellings for each of them. Until now, a model of the cochlea including all of these phenomena has not appeared in the literature. For this reason also in this thesis the cochlear partition, except for the basilar membrane (BM), is not modelled: it is assumed that its influence on overall fluidodynamic processes of scala vestibuli and scala tympani is negligible.

The immersed boundary method is widely used for biofluid-dynamics modelling. It solves in a satisfying way the problem of implementation in fluid fields of thin elements (membranes) with articulated shapes. As a consequence, in this study the BM has been implemented in the cochlea with this technique.

The basilar membrane is modelled as a set of oscillators described by:

$$m \frac{\partial^2 \eta}{\partial t^2} + r \frac{\partial \eta}{\partial t} + K \eta = F, \quad (3.1)$$

3.1. Computational model of the cochlea

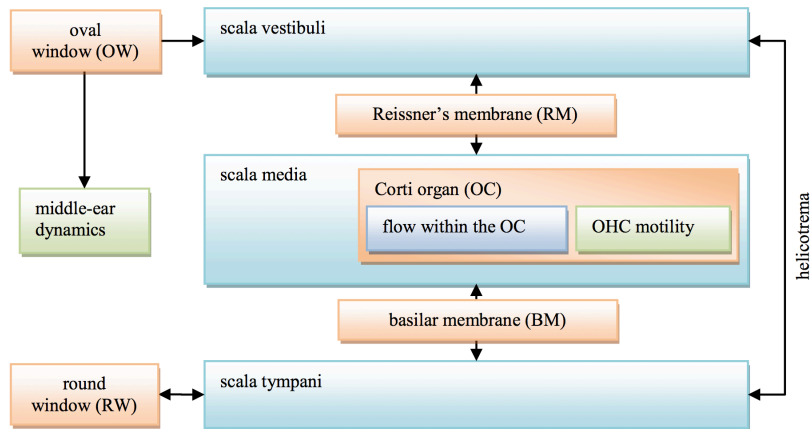


Figure 3.2: Schematic of the interactions between the components and processes of the cochlea (OHC is the acronym for outer hair cells)[2].

where η stands for BM's point displacement, m , K , r for, respectively, its mass, stiffness and damping, t for time and F is the force that the fluid exerts on the point (by the means of differential pressure through the membrane in that point). In this model m and r are supposed to be vanishingly small, this is justified if it is assumed that inertia and damping are dominated by the fluid. It must be noticed that with this relation it is implicitly assumed that the *membrane elements are not mechanically coupled*, i.e. each point is not interconnected with the points in the vicinity, as η is the absolute displacement and not the displacement relative to the neighbouring points. As a result, the intra-membrane forces are modelled through a *coupling of each point with its resting position*.

Each point of the BM is assumed to exerts a force on the fluid on both longitudinal and transversal direction. If we set a coordinate reference system, with the x -direction along the lenght of the cochlea and the y -direction along its height (see fig. 3.1), with the assumed hypotheses, the

equations for the BM can be expressed in the following way:

$$\begin{aligned} k_x \eta_x &= f_x, \\ k_y \eta_y &= f_y. \end{aligned} \tag{3.2}$$

It must be noticed that these relations are basically eq. 3.1, but per unit length of the cochlea. This means that:

$$\begin{aligned} f_x &= \Delta p_x, \\ f_y &= \Delta p_y, \end{aligned} \tag{3.3}$$

where Δp_x stands for the pressure difference across the membrane in the x -direction, and Δp_y for the pressure difference along y -direction.

Finally, the stiffnesses of the membrane along both directions are assumed to vary along x with the following relations ([5]):

$$\begin{aligned} k_x(x) &= k_0 e^{-\left(\frac{x}{2A}\right)}, \\ k_y(x) &= k_x(x) \cdot 10^{-2}. \end{aligned} \tag{3.4}$$

where:

$$A = 1.30288... \cdot 10^{-3} \text{ mm}, \tag{3.5}$$

and:

$$k_0 = 3.255... \cdot 10^9 \frac{N}{m^3}. \tag{3.6}$$

These coefficient come from experimental measurements in dead cochleas.

Finally the round window (RW) stiffness is assumed to be null. Much research on this topic has shown that the RW impedance does not have effect on the overall cochlear dynamics, for this reason it has been decided to set the RW stiffness to zero. As a consequence, RW is assumed to behave like an hole placed in the walls of the cochlea.

3.2 Solution procedure

It has been stated previously that the basilar membrane is implemented with the immersed boundary method. This means that in the computational model there are two grids: one *Eulerian grid for the flow*, and one

3.2. Solution procedure

Lagrangian grid for the basilar membrane, and that the two grids are coupled with the process showed in the flowchart of fig. 3.3.

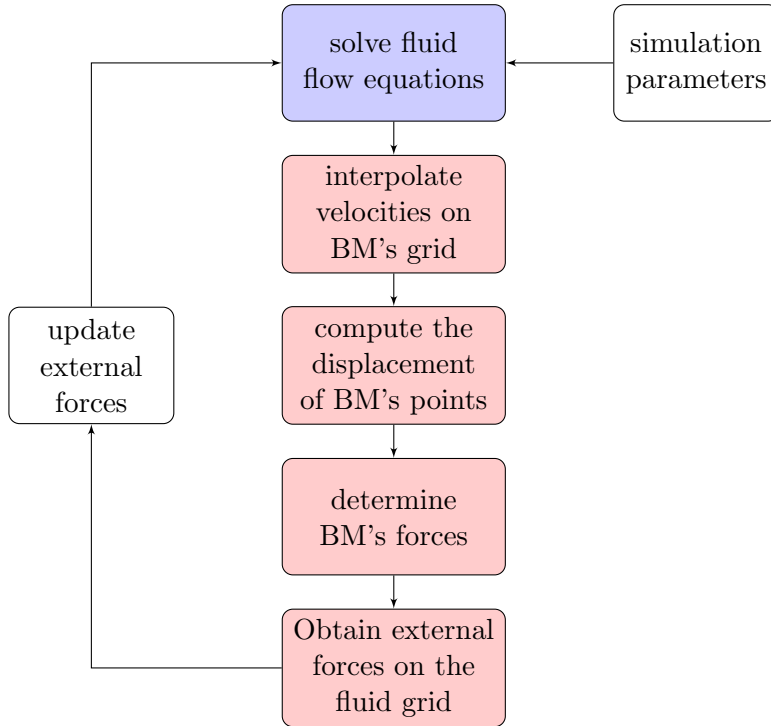


Figure 3.3: Flowchart of the solution procedure.

It must be noticed first, that the code works with an iterative process. Starting with a zero field of external forces, through a certain number of iterations (usually each time-step in the simulations carried out in this thesis required a number between 7 and 13 iterations) the code reaches convergence and gives a solution for the particular time considered. As suggested by the color of fig. 3.3 the phases written in the red boxes can be interpreted as a unique step which can be addressed to as *computation*

of external forces on fluid grid; they specifically deal with the problem of implementation of membrane forces on the fluid field. The blue box indicates instead the processes related with fluid motion. The remaining part of this section will explain in more details each phase of the simulation process.

3.2.1 Simulation parameters

It is first necessary to describe what parameters are known, and how they are implemented in the code. The known parameters are:

- cochlear box configuration,
- membrane properties and fluid properties,
- discretization characteristics, both in time and space,
- temporal extent of the simulation,
- movement of the oval window (OW) in time,

each of them is examined below in more detail.

Cochlear box configuration

Several configurations of the cochlea have been simulated, each of them will be explained later in this chapter. There some features common to all the simulations: the oval window (OW) position, length and height of the box. These features are depicted in fig. 3.4. The walls of the box are assumed to be infinitely rigid. As showed in the figure, the length and the height of the cochlear box are supposed to be, respectively, 36 and 1.44 mm, these are the dimensions of a mean human cochlea [1]. The figure shows also the coordinate system used for the simulations: the origin is placed at the left-lower corner of the box, the x -direction runs along the length of the cochlea while y along its height. The oval window is placed in the upper wall, the distance between its left edge and the upper-left corner of the box is $0.6mm$. The dimension of the oval window in these simulations

3.2. Solution procedure

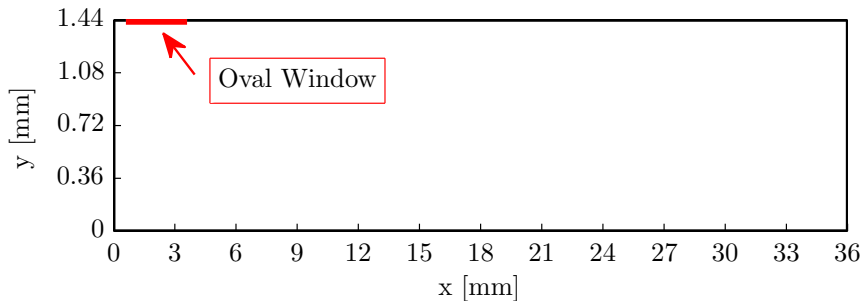


Figure 3.4: Box features common to all the simulations

is supposed to be 3 mm, as human oval windows have a size between 2.9 and 3.3 mm [1].

Membrane and fluid properties

As damping and mass of the BM are supposed to be zero, the only property needed for the simulation is the distribution of the stiffness along BM's length, which is known by eq. 3.4.

As for the fluid, it was already said that the perilymph is supposed to behave like water.

Discretization characteristics

To start the computation it is necessary to define a space grid on which the fluid flow equations are solved. Actually the user has to define three grids, the pressure grid, and two grids for the two components of the velocity, because the flow solver works with a staggered grid (see 3.2.2). Different configurations for the grid were used for the simulation, each of them will be specified for every case.

The definition of time discretization is not decided directly by the user: the flow solver works with a step time that is defined once both the space grid and a value for the CFL number is chosen. More explanation about

this aspect can be found in sec. 3.2.2.

Temporal extent of the simulation

The simulations are run for 25 periods of OW oscillations, in which the travelling wave on the membrane is assumed to reach a steady state.

Movement of the OW

In these simulations it is assumed that the movement of the stapes, i.e. the movement of the oval window in time, is known. In this model the OW's velocity is defined through the following parameters:

- the frequency of its oscillation,
- its maximum velocity,
- the oscillation amplitude variation during the numerical simulation.

The frequency and the maximum velocity are varied during the simulations, their value will be specified each time. During the first 12 periods of simulation, the inflow velocity at the stapes is ramped as showed in fig. 3.5.

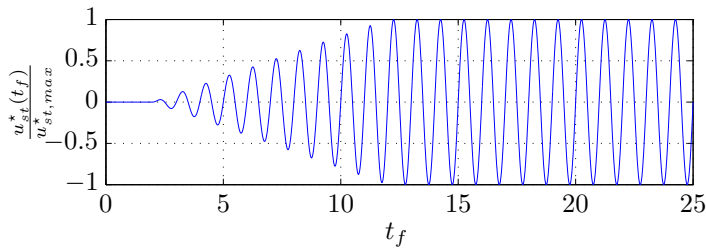


Figure 3.5: Non-dimensional velocity of the oval window plotted as a function of non-dimensional time.

In the figure, t_f is a non-dimensional time of simulation, non-dimensionalized with the period of oscillation of the OW, $u_{st}^*(t_f)$ is the actual velocity of

3.2. Solution procedure

the OW, and $u_{st,max}^*$ is the maximum velocity reached by the OW when a (statistically) steady state is reached.

3.2.2 Solver for fluid flow equations

”IMPACT” is the numerical framework which solves an adimensional form of the Navier-Stokes equations for incompressible flows. Further details on this code can be found in [6], this section of the chapter goes through its main features.

Scales for non-dimensionalization

As the code works with non-dimensional equations, to start the computation it is necessary to define a number of scales that will be applied to all dimensional parameters of the problem. From this point of the thesis on, a convention will be followed: the letters with a star (\star) will mark dimensional parameters, whereas the letters without will indicate an adimensional parameter. The scales chosen for the simulations carried out for this project are the following:

- a length scale: L_{char}^* ,
- a velocity scale: u_{char}^* ,
- a time scale: $t_{char}^* = \frac{L_{char}^*}{u_{char}^*}$;
- a pressure scale: $p_{char}^* = \rho^* (u_{char}^*)^2$.

Non-dimensional equations

The IMPACT code operates solving Navier-Stokes equations in dimensionless form [6]

$$\frac{\partial \mathbf{u}}{\partial t} + (\mathbf{u} \cdot \nabla) \mathbf{u} = -\nabla p + \frac{1}{Re} \nabla^2 \mathbf{u} + \mathbf{f}_{ext}, \quad (3.7)$$

combined with the continuity equation:

$$\nabla \cdot \mathbf{u} = 0. \quad (3.8)$$

The adimensional quantities of equations 3.7 and 3.8 can be easily obtained with the scales defined above. The adimensional velocity is defined as:

$$\mathbf{u} = (u, v) = \left(\frac{u^*}{u_{char}^*}, \frac{v^*}{u_{char}^*} \right), \quad (3.9)$$

whereas the adimensional pressure is:

$$p = \frac{p^*}{\rho^* (u_{char}^*)^2}, \quad (3.10)$$

and the Reynolds number is:

$$Re = \frac{u_{char}^* L_{char}^*}{\nu^*}, \quad (3.11)$$

where ν^* is the viscosity of the fluid. In fact, the program needs also the definition of three other adimensional numbers, i.e. the Womersley number which is defined as:

$$\alpha = L_{char}^* \sqrt{\frac{\omega^*}{\nu^*}}, \quad (3.12)$$

the adimensional Stokes boundary layer thickness, given by the expression:

$$\delta_S = \frac{\delta_S^*}{L_{char}^*}, \quad (3.13)$$

and a non-dimensional frequency:

$$f = f^* t_{char}^*; \quad (3.14)$$

in the relations above, ω^* is defined as $\omega^* = 2\pi f^*$, and f^* represents the OW's frequency of oscillation.

3.2. Solution procedure

Computational grid and discretization

To avoid stability problems that would arise if the grid chosen for the computations were a collocated grid, the IMPACT code discretizes and solves the equations implementing finite differences on a *staggered grid*. This means that the primary unknowns, i.e. the velocity (u, v) and the pressure (p) are sought at different points in the grid, or better, we can see the overall grid as composed of three different grids, each of them is "specialised" for one of the three primary unknowns (see fig. 3.6). The mo-

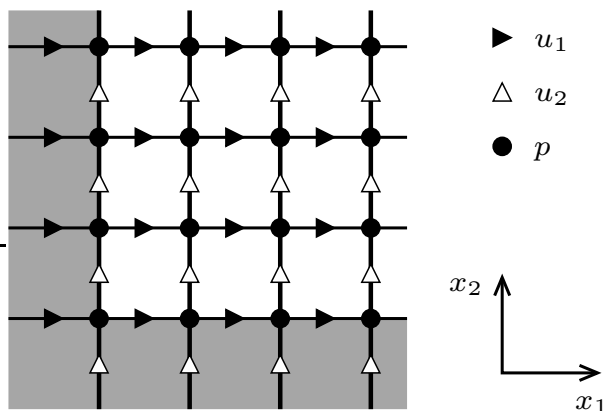


Figure 3.6: Staggered grid in two dimension next to the boundaries, where: $x_1 \equiv x$, $x_2 \equiv y$, $u_1 \equiv u$ and $u_2 \equiv v$.

mentum equations are solved on the respective velocity grids, the continuity equation is satisfied on the pressure grid.

The spatial discretization is done, on this staggered grid, using finite differences of order 6 (thus the approach is 6th order accurate in space).

Boundary and initial conditions

To obtain a numerical solution, *boundary conditions* and *initial conditions* for the velocity are required. Indeed, due to the specific structure of

the Cartesian staggered grid, only the velocity needs boundary and initial conditions. The application of boundary and initial conditions is done in the following way:

- the boundary conditions for the velocity are implemented as Dirichlet boundary conditions which impose zero velocity at the walls of the cochlear box and in and out-flow velocity at the oval window of the cochlear model. At the round window the flow is imposed in a way that it balances the flow term from the oval window: as the fluid is incompressible, the fluid volume deficiency/excess caused by oval window movement has to be balanced by an equal excess/deficiency of fluid volume at the round window;
- the initial condition is defined imposing a zero velocity thorough the cochlea at $t = 0$.

Time integration

The solution for the flow is computed iteratively. A system of linear equations (obtained with a discretization of eq. (3.7) and (3.8)) has to be solved at each sub-timestep during time integration. Indeed, the equations are solved by a three stage *3rd order Runge-Kutta method* (3rd order accurate in time). The code is parallelized so that it can be run on different processors, for efficiency reasons. The timestep used to solve the equations is chosen in an indirect way; instead of (Δt) (i.e. temporal resolution), the user has to set a number, called CFL number (where CFL is an acronym defined by the first scientists that suggested this procedure, Courant-Friedrichs-Lévy). The CFL number determines the condition that has to be fulfilled to ensure the stability of the numerical solution of partial differential equations when using a finite differences method, this condition is:

$$\frac{\Delta t}{\Delta x} u + \frac{\Delta t}{\Delta y} v \leq CFL, \quad (3.15)$$

where Δx and Δy are the mesh-widths respectively in x and y direction. In the IMPACT framework, the definition of CFL is slightly different due

3.2. Solution procedure

to normalisation of the equation (see [6] for further details). As we can see from eq. (3.15), the CFL specifies a maximum time-step size, which is the maximum Δt allowed in order to ensure convergence of the method.

3.2.3 Computation of external forces on the fluid

Once a solution of the flow is found, it is necessary to update the forces of the BM, that can now be computed as the velocity is known on the fluid grid. The process to obtain the forces to apply in the fluid can be developed in different steps, showed below.

Before starting, we need first to define the interpolation function δ : as explained in (2.3) it is essential to switch from one grid to another. In the code developed in this work δ is defined in the following way:

$$\delta = \delta_x(r_x)\delta_y(r_y) \quad (3.16)$$

$$\begin{cases} \delta_h(r_h) = \frac{\Delta_h - |r_h|}{\Delta_h^2}, & \text{if } |r_h| \leq \Delta_h; \\ \delta_h(r_h) = 0, & \text{if } |r_h| > \Delta_h; \end{cases} \quad (3.17)$$

where

$$h = x, y;$$

r_h is the distance from the BM's point considered along the h -direction, Δ_h is the mesh width of the Eulerian grid along the h -direction. This interpolation function involves only the *four* points at the vertices of the cell in which the BM point considered lies.

The steps to compute BM's forces are itemized below (see fig. 3.3, steps in the red boxes).

1. *Interpolate velocities on BM's grid*; writing:

$$\mathbf{r} = \mathbf{x} - \mathbf{X}(s, t) \quad (3.18)$$

it is possible to lead back to the δ function defined previously in eq. (2.4). Then a discretization of eq. 2.4 to find the velocity on the Lagrangian grid is performed.

2. *Compute the displacement of the BM's points*; once that the velocity on the BM's grid are found, a third-order Runge-Kutta integration is used to obtain the displacement of each point on the grid.
3. *Determine BM's forces*; once that the displacement of each point is known, a discretized version of eq. (3.2) is used to obtain the BM's forces per unit length. It must be noticed that eq. (3.2) is eq. (2.1), where A_f has been specialized for our particular problem.
4. *Obtain external forces on the fluid grid*; through another interpolation, achieved discretizing eq. (2.2), it is possible to obtain the external forces applied by the membrane on the fluid grid. These forces will be used to start again the process of computation from the beginning step until convergence.

3.3 Constant OW's velocity simulations

Now that a general description of the code has been provided, it is possible to proceed describing the different configurations used in the course of this thesis.

The first batch of simulations was run to study a new cochlear box configuration. The classical box layout used to model the cochlea, which in this work is named "base configuration", was not adequate to describe the fluid flux next to the RW. For the purpose of this thesis, it is instead crucial to have a good reproduction of the flux around the RW. The microphone model will be inserted right beside the round window; as a consequence the flow characteristics in that region has to be modelled as precisely as possible to have good indications for microphone optimal place and its influence on the overall dynamic of the cochlea.

In this chapter three configurations are described:

- *base configuration*, as already said is the layout of cochlear box most utilized to simulate cochlear dynamics;

3.3. Constant OW's velocity simulations

- *configuration with moved RW*, to inspect separately the effects of each change in the configuration, an intermediate arrangement has been inspected;
- *proposed configuration*, this configurations is believed to simulate very precisely (considering the limits of a 2-D model) the flux next to the RW.

Before starting with a description of the three configurations, it is necessary to see the common parameters used when running these simulations. As suggested by the title of this section, the maximum OW's velocity amplitude of oscillation was kept constant through all the cases studied; on the contrary the frequency of OW's oscillation has been varied between 500 Hz and 4 kHz, to study its effects on the different configurations. The scales used were the same for all the simulations:

– *length scale*: $L_{char}^* = 3 \cdot 10^{-3} \text{ m}$,

which is the assumed length of the OW;

– *velocity scale*: $u_{char}^* = 3 \cdot 10^{-5} \frac{\text{m}}{\text{s}}$,

which is the velocity amplitude of oscillations of the OW, whose value was decided to optimize the efficiency of computation [5]; from these two scales it is easy to obtain the remaining two, i.e.

– the *time scale*: $t_{char}^* = 10^2 \text{ s}$ and

– the *pressure scale*: $p_{char}^* = 3 \cdot 10^{-2} \text{ Pa}$.

Finally, for these simulations a value of $CFL = 0.25$ was set. Sufficient resolution of spatial and temporal discretization is crucial for stability and accuracy of the simulations. A small value of the CFL results in small time step size. In this project this value has been set in order to reach a good trade-off between two factors; if the CFL is too high the simulation runs with a big time step but at each step there is the need of many iterations to reach convergence; on the other hand if the CFL is too low, every step needs less iterations but the simulations run slowly due to the low Δt size.

3.3.1 Base configuration

Fig. 3.7 shows the arrangement of the *base configuration*.

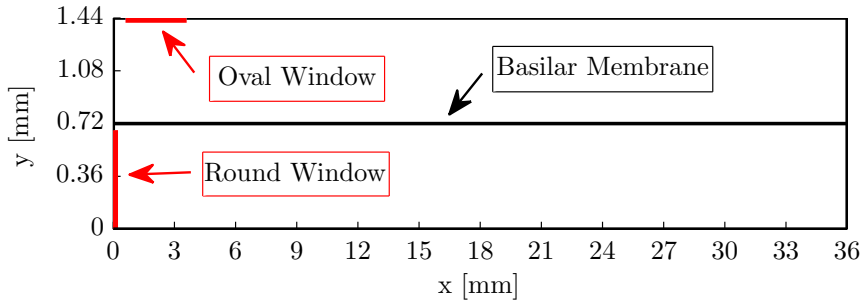


Figure 3.7: Box arrangement of base configuration.

The figure illustrates that the basilar membrane is flat, and it is located at half height of the cochlea: in this way it divides the cochlea into two perfectly equal canals, which should model the Scala Vestibuli and the Scala Tympani. The round window is placed on the left side of the box, its length in this configuration is 0.675mm .

The fluid pressure grid for this configuration has the following characteristics:

- equally spaced along x , with 3073 points and a resulting step $\Delta x = 0.0117.. \text{mm}$;
- not equally spaced along y , with 97 points, in a way that the grid is coarse in the centre of the canals and fine next to the Lagrangian points and to the wall: results $\Delta y_{min} = 0.006189.. \text{mm}$ and $\Delta y_{max} = 0.02422.. \text{mm}$.

A grid portion of one of the two canals (precisely the scala tympani) is shown in fig. 3.8, the grid in the scala vestibuli has the same shape. The u and v -velocity grids can be easily obtained from the pressure grid shifting it in space.

3.3. Constant OW's velocity simulations

The Lagrangian grid has one point per each fluid cell, this means that there are 3073 points to model the membrane.

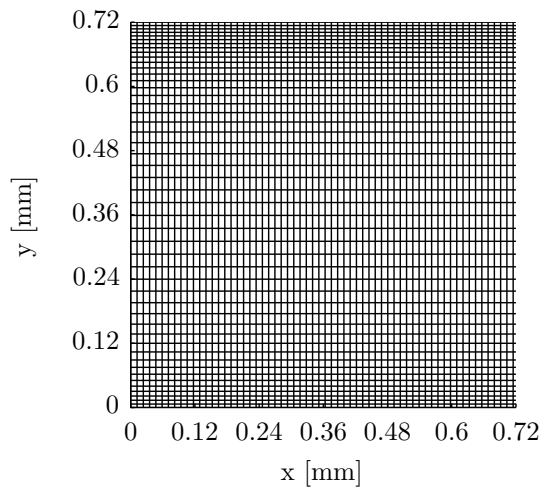


Figure 3.8: Portion of the grid implemented for the base configuration.

3.3.2 Problems of the base configuration

Three problems of the base configurations must be highlighted:

- the round window on the left side of the box instead of at the bottom side,
- round window length is much shorter (about one fourth) of the RW in a real human cochlea,
- the "hook region" of the cochlea is not modelled.

To discuss about these problems, it is useful to look at fig. 3.9, which shows a depiction of the cochlea; in the vicinity of the RW there is a hole in

the wall of the cochlea, to display the *hook region* of the cochlea. The hook region is a fraction of the cochlea, next to the RW, where the BM curves, like a hook, towards the RW. The base configuration does not model the

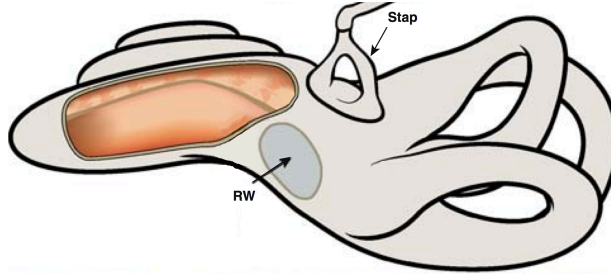


Figure 3.9: Cochlea layout ("RW" stands for round window, "Stap" for stapes)[17].

hook region of the cochlea, as the BM is supposed to be flat. Moreover the RW is supposed to be on the left side of the box, when the RW should be placed instead in the bottom side of the box; finally the length of the RW in this configuration is limited by the height of the semi-canal of the cochlea, thus the size imposed to the RW is one third of the length of the RW in a real human cochlea. These features of the base configuration make us understand that this layout of the box does not give accurate pressure fields in the region of the RW.

3.3.3 Configuration with moved RW

The second configuration implemented has the RW in the bottom side of the box. As there are no limitations to its size in this place, the RW has been enlarged in order to model better its size in a human cochlea [1]. As a consequence, in the model proposed a RW's length of 2.4 mm was chosen. The left side of the RW is placed exactly at the lower left corner of the box. The BM in this configuration has the same shape of the BM in the base configuration, i.e. a flat shape. In fig. 3.10 all the features of the new box arrangement are displayed.

3.3. Constant OW's velocity simulations

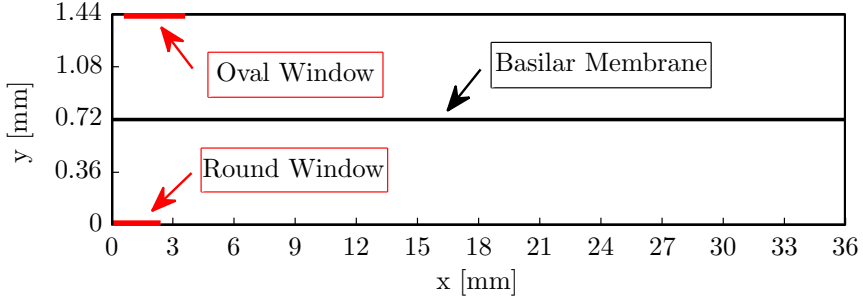


Figure 3.10: Box configuration with moved RW.

The fluid grid for this configuration is the same used for the base configuration, also the BM's grid was not changed.

3.3.4 Proposed configuration

To keep in account of the hook region, the last configuration has been modified. The resulting configuration is the one proposed as possible new box arrangement for the future studies on the cochlea.

The implementation of the curve in the BM has been developed imposing the shape described by the following rule:

$$y_{BM}(x) = Y_{BM}(1 - e^{\frac{x}{X_{\tau}}}) + Y_{0,BM}, \quad (3.19)$$

where:

$$Y_{BM} = 0.72 \text{ mm}, \quad (3.20)$$

is the height where the BM is hinged at the right side of the box;

$$Y_{0,BM} = 0.036 \text{ mm}, \quad (3.21)$$

is the height where the BM is hinged at the left side of the box, and

$$X_{\tau} = 1.8 \text{ mm}, \quad (3.22)$$

is the space constant of the exponential law (3.19) ; it represents the value of x where the BM has an height equal to the 63.2% of its asymptotic value (i.e. Y_{BM}). In fig. 3.11 the initial part of the BM resulting from this equation, with a 1 : 1 aspect ratio of the axes is depicted.

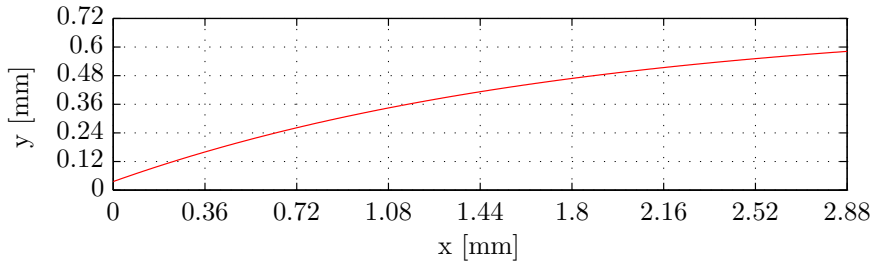


Figure 3.11: Membrane shape resulting from eq. 3.19 with a 1 : 1 aspect ratio of the axes.

Concerning the RW, it has been placed in the same location and with the same size as the configuration described in 3.3.3. Besides, the effect that a rightwards shifting of the RW has on the dynamic of the cochlea has been studied. Precisely, three positions of the RW have been tested:

- *case 1*, left edge of the RW at the left-lower corner of the box (see fig; 3.1). This is the configuration that will be used for the implementation of the microphone model;
- *case 2*, left edge of the RW at a distance of 0.75 mm from the left lower corner of the box (see fig. 3.12);
- *case 3*, left edge of the RW at a distance of 1.5 mm from the left-lower corner of the box (see fig. 3.13); this is the same distance that there is between the left edge of the OW and the upper left corner.

It can be noticed that these configurations, with the shape of the basilar membrane imposed, have the two canals (vestibular and tympani canal) considerably different in shape in the beginning part of the cochlea, in agreement with the real shape of the human cochlea (cf. again fig. 3.9).

3.3. Constant OW's velocity simulations

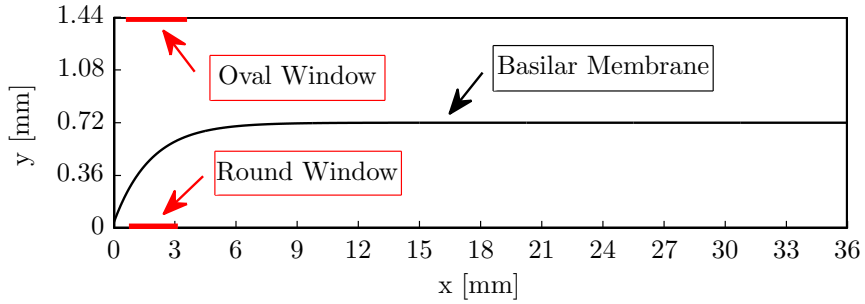


Figure 3.12: Case 2, distance of 0.75 mm between the RW and the corner.

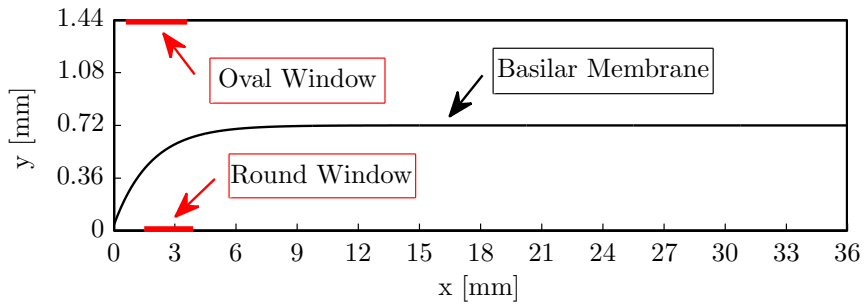


Figure 3.13: Case 3, distance of 1.5 mm between the RW and the corner.

The grid for the discretization of these box has been changed from the configuration described in 3.3.1, in order to have *a fine resolution next to all BM's points*. The pressure grid used to discretize these configurations of cochlear box (i.e. both case 1, case 2 and case 3) has the following characteristics:

- equally spaced along x , with 3073 points and a resulting step $\Delta x = 0.0117.. mm$;
- equally spaced along y in the lower half of the cochlea, with 121 points and a resulting step $\Delta y = 0.006 mm$;
- not equally spaced along y in the upper half of the cochlea, the distribution is the same shown in fig. 3.8, this means that in the upper half of the cochlea there is the same grid used for the tympanic canal in the base configuration.

Stability problems arised with the new shape of the BM. Remarkable discontinuities and peaks of the velocity and the pressure across the membrane were observed. To solve these problems it was necessary to change also the grid used to follow the movement of the BM. In 3.3.1 it was explained that in the base configuration there is one BM's grid point per each fluid cell, this results in a first order accuracy of forces computation. To increase the order of accuracy it has been implemented a layout of the grid in which there are two membrane points per each fluid cell. As a result, the new BM's grid includes 6145 points for the computation of BM's forces.

Finally, a last modification was necessary in the process of computation of the forces on the BM. In equations (3.2), the stiffness along x and y can be expressed with the relations (3.4) only if the membrane is flat and aligned with x . In this configuration the first portion of the BM is not flat, the stiffness has thus to be expressed in another way. First is necessary to define a *local reference system* with axes (t, n) : t is the direction of the axis locally tangent to the membrane, n is the direction of the axis locally normal to the membrane. Once that this local reference system is defined,

3.3. Constant OW's velocity simulations

it is possible to write:

$$\begin{aligned} k_t \eta_t &= f_t, \\ k_n \eta_n &= f_n. \end{aligned} \tag{3.23}$$

η , f and k are, respectively the displacement, the force and the stiffness of the BM's points. As suggested by the subscripts they are computed on local coordinates. With this approach it is now possible to utilize the equations (3.4), but reshaped in the following way:

$$\begin{aligned} k_t(s) &= k_0 e^{-\left(\frac{s}{2A}\right)}, \\ k_n(s) &= k_t(s) \cdot 10^{-2}, \end{aligned} \tag{3.24}$$

where s is the arclength of the membrane, k_0 and A are expressed, respectively, by equations (3.6) and (3.5).

It must be noticed that when the BM's displacements are computed through the interpolation from the velocity grid, η_x and η_y are obtained. To attain the displacements in local coordinates there is the need for the following equations:

$$\begin{aligned} \eta_t &= \eta_x \cos \alpha + \eta_y \sin \alpha, \\ \eta_n &= -\eta_x \sin \alpha + \eta_y \cos \alpha, \end{aligned} \tag{3.25}$$

where α has been obtained from:

$$\alpha = \arctan \left(\frac{\partial y_{BM}}{\partial x} \right) \tag{3.26}$$

$y_{BM}(x)$ is expressed by eq. (3.19). Once that the forces are obtained with equations (3.23), through another rotation of the coordinate system it is possible to obtain the forces on the global reference system:

$$\begin{aligned} f_x &= f_t \cos \alpha - f_n \sin \alpha, \\ f_y &= f_t \sin \alpha + f_n \cos \alpha. \end{aligned} \tag{3.27}$$

3.4 Comparison with experimental results

Once that the features of the new configuration have been studied, a comparison was carried out with the experimental results to verify if the set-up proposed is actually more accurate next to the RW. To make the comparisons with the experimental results, only two of the five configurations presented in the previous section were run; i.e. the one explained in 3.3.3 and *case 1* of 3.3.4. Before explaining the procedure followed to make the comparison with the experimental results, it is necessary to go briefly through the papers [17] and [16] used as a reference for the experimental results.

3.4.1 Results of Nakajima et al. [17]

A rendering of the measurements carried out by Nakajima et al. is showed in fig. 3.14. The experimenters measured the pressure at the scala

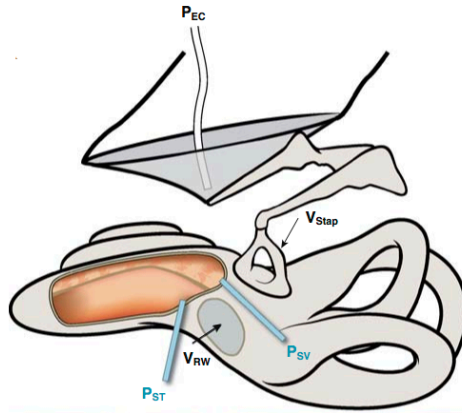


Figure 3.14: Illustration showing the locations of various types of recordings carried out by Nakajima: pressure in scala vestibuli (P_{SV}), pressure in scala tympani (P_{ST}), pressure in the ear canal (P_{EC}), velocity of the stapes (V_{Step}), velocity of the round window (V_{RW}) [17].

tympani and the pressure at the scala vestibuli at different frequencies of

3.4. Comparison with experimental results

stimulation of the cochlea. They carried out their observations on 7 different dead human cochlea. As shown in the picture they also measured the stapes velocity (they did not measure the round window velocity, but they supposed that it was equal to the velocity of the stapes): this was necessary to correct the values of the pressure found with the pressure sensors, since there is a relationship between the cochlear sound pressure and the stapes volume velocity. The experimenters normalized the values of the pressure found with the eardrum pressure values (i.e. p_{EC} in fig. 3.14) measured through the sensor placed in the tympani.

It must be noticed that in this work the interest is focused on the pressure measurements in the scala tympani, because the measurement points were placed exactly in the vicinity of the RW, i.e. the region where the model of the microphone will be located. In the paper they carried out the simulations on 7 cochlea, the pressure measurements in the scalae can be shown either separately for each cochlea, or using a statistical approach, plotting one curve for the mean and two curves that circumscribe the strip in which the results lie. Fig. 3.15 displays the results from Nakajima et al., with the latter approach to show the data, normalized with the pressure on the eardrum and expressed in decibel.

3.4.2 Results of Sim et al. [16]

The aim of the work by Sim et al. [16] is to measure the velocity of the stapes in six dead human cochlea, when the tympani is stimulated by a pressure signal. The magnitude of the pressure on the eardrum is again measured with a pressure sensor located on the tympani.

The results are shown in fig. 3.16, where the mean magnitude of the translational velocity at the footplate center is plotted versus the frequency of oscillation of the eardrum. In the figure the maximum possible error ($|v_{OZ}|_{MPE}$) in the measure of the velocity is also plotted. As the velocities are normalized with the pressure at the eardrum, the units of the velocity magnitude are: $\frac{mm}{s \cdot Pa}$.

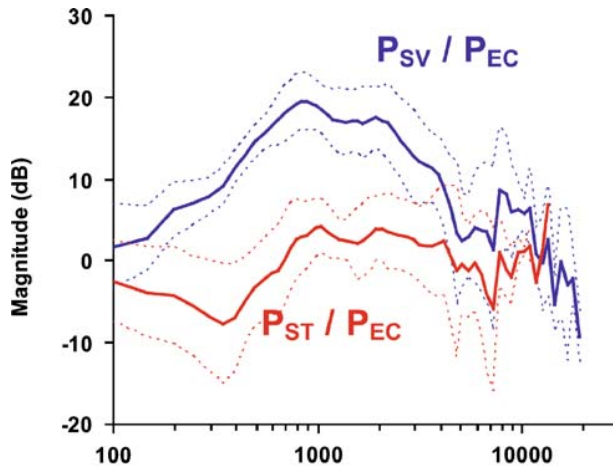


Figure 3.15: The means and standard deviations of the pressures in scala vestibuli and scala tympani relative to the ear canal pressure [17].

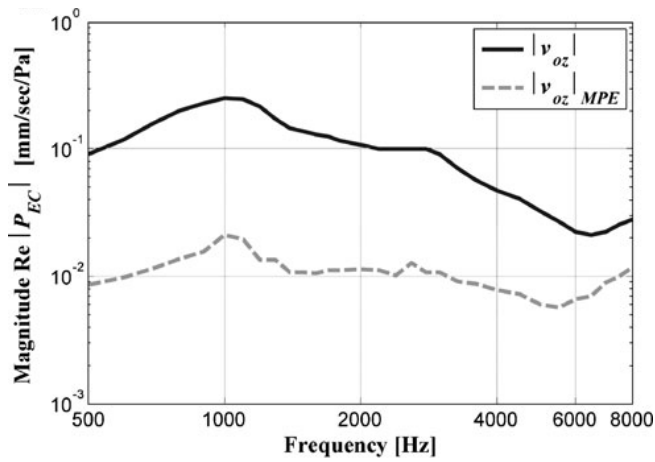


Figure 3.16: Mean magnitude of the translation velocity at the footplate center ($|v_{OZ}|$), and its maximum possible errors $|v_{OZ}|_{MPE}$ [16].

3.4. Comparison with experimental results

3.4.3 Procedure for the comparison

The procedure used to make the comparison is shown schematically in fig. 3.17. In the middle of the figure (circles and straight arrows that link

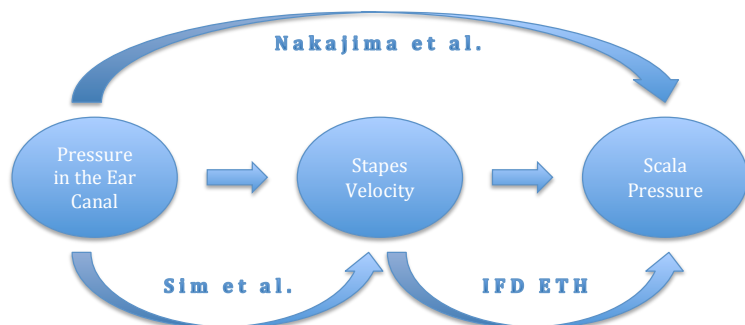


Figure 3.17: Procedure followed for the comparison with experimental result, "IFD ETH" is the numerical code implemented in this work.

them), the process as it is in nature is displayed (see 2.1). In the upper part of fig. 3.17 the way in which the Nakajima's results were found (i.e. imposing the pressure at the eardrum, measuring the pressure in the scala tympani and in the scala vestibuli) is depicted, whereas in the lower part the way in which the numerical data to be compared were found is shown. The numerical code implemented in this work receives as input the velocity of the OW, on the other hand Nakajima results were found imposing the pressure at the eardrum. To make the comparison Sim's relation between the pressure at the eardrum and the velocity at the footplate of the stapes (which is equal to the velocity of the OW) was used; as a consequence also in the lower part a relation between the pressure in the ear canal and the pressure in the scalae is obtained.

For the comparison only two box configurations were used, i.e. the ones depicted in fig. 3.10 and in fig. 3.1. Each of them was tested at four different frequencies. The frequencies chosen for the simulations are:

500 *Hz*, 1 *kHz*, 2 *kHz* and 4 *kHz*. The velocities imposed at the OW (as explained they were assumed using the results from Sim et al., see fig. 3.16) for the different frequencies are:

$$\begin{aligned}
 f^* = 500 \text{ Hz} &\rightarrow u_{stapes}^* = 0.9 \cdot 10^{-4} \frac{m}{s}, \\
 f^* = 1 \text{ kHz} &\rightarrow u_{stapes}^* = 2.5 \cdot 10^{-4} \frac{m}{s}, \\
 f^* = 2 \text{ kHz} &\rightarrow u_{stapes}^* = 1.05 \cdot 10^{-4} \frac{m}{s}, \\
 f^* = 4 \text{ kHz} &\rightarrow u_{stapes}^* = 4.8 \cdot 10^{-5} \frac{m}{s}.
 \end{aligned} \tag{3.28}$$

The velocity scale for each simulation is different as it is defined in the following way:

$$u_{char}^* = u_{stapes}^*, \tag{3.29}$$

while the values for the length scale and CFL are preserved as defined in 3.3.

Once the parameters of the code are set, and the simulation has run, the position where the pressure is computed in the cochlear box should be decided. It is hard to define in the model the precise location of the sensors placed in Nakajima's measurements. The only thing that is known, is that the sensor penetrates next to the RW (see fig. 3.18, P_{ST} is the sensor of our interest), and that its position in the cochlea has been estimated to be around 0.2 *mm* far from the wall in which the RW lies (see [17]).

As a result for this uncertainty on the pressure sensor location, three measurements points for the pressure have been located in each of the two boxes, at different distances from the RW. As the penetration in the cochlea is known, the points are set all at the same height. Fig. 3.19 and fig. 3.20 show the location of the three measurement points ('x' markers in cyan) in the box configurations tested.

It must be noted that, following this procedure, the cochlear response when the ear is stimulated by a 1-Pa-amplitude pressure wave on the eardrum, is substantially tested.

Finally, the comparisons with Nakajima's results are obtained carrying

3.4. Comparison with experimental results

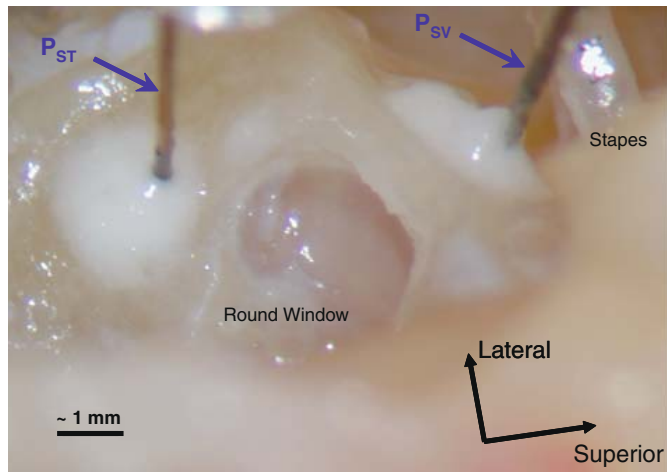


Figure 3.18: Photograph of left temporal bone showing pressure sensors inserted into scala vestibuli (P_{SV}) and scala tympani (P_{ST}).

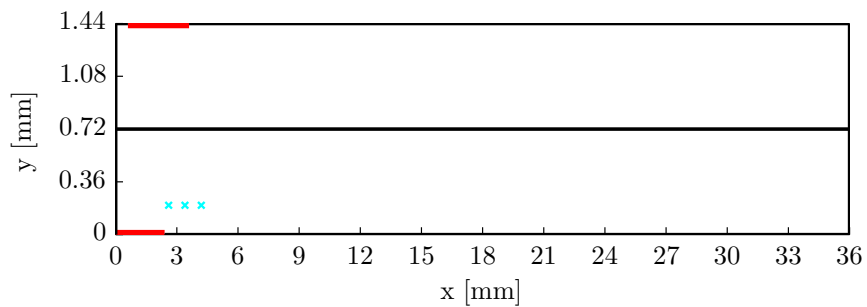


Figure 3.19: Measurement points ('x' markers in cyan) in the first box configuration tested.

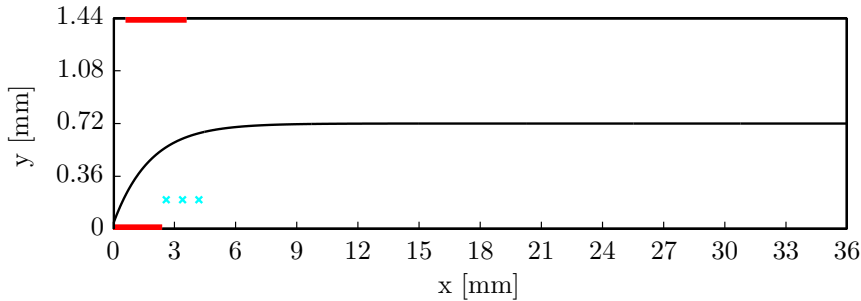


Figure 3.20: Measurement points ('x' markers in cyan) in the second box configuration tested.

out measurements on dead cochleas. This is a favorable condition because in the computational model presented the active processes are not considered.

3.5 Configuration with the microphone

The last step of this work focused on the implementation of the microphone in the cochlear box. The application of the microphone has been divided into two stages: in the first one a hole was made in the cochlear box and, through this hole, the microphone model has been inserted in a second instance. The modifications have been implemented in the configuration showed in fig. 3.1, i.e. case 1 in 3.3.4.

For these two configurations only two simulations were run, one for each box arrangement. Just one frequency was tested, i.e. 1 kHz , with a OW's velocity of $u_{stapes}^* = 2.5 \cdot 10^{-4} \frac{m}{s}$ and this velocity was chosen as velocity scale, while the length scale and CFL are the same used for the other simulations.

3.5.1 Cochlear box with the hole

The microphone model has been implemented right next to the RW. For practical reasons, the intra-cochlear receiver cannot be placed too far from

3.5. Configuration with the microphone

the RW. As the signal just above the RW is really low (this will be shown in the following chapters), the microphone cannot pass through the RW. As a result, a reasonable location that reaches a good compromise between amplitude of the signal and surgical ability to place it, is right next to the RW.

Considering the location of the microphone, the hole has been made next to the RW. Fig. 3.21 illustrates the resulting cochlear box.

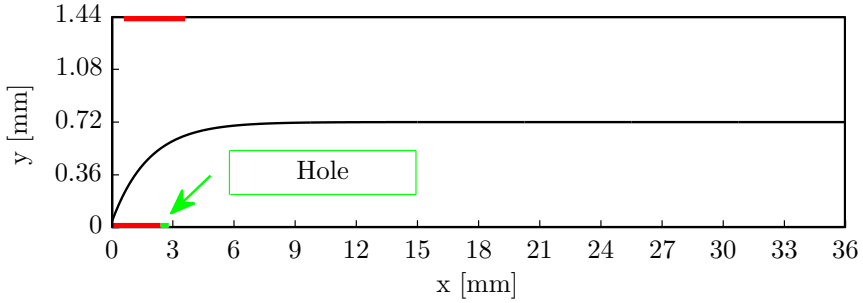


Figure 3.21: Box configuration with the hole next to the RW.

The length of the hole is 0.4 mm (this is the width of the microphone model proposed in [18]), its left edge is 2.4 mm far from the lower left corner of the box; as a result the right edge of the RW and the left edge of the hole are in the same point.

The implementation of the hole in the code was relatively straightforward, the boundary conditions were changed, imposing in this case that the mass flow rate at the OW was equal to the sum of the mass flow rate of the RW and the mass flow rate of the hole, i.e.:

$$\dot{m}_{OW} = \dot{m}_{RW} + \dot{m}_{hole}. \quad (3.30)$$

It was not necessary to change either the BM's grid nor the fluid grid.

Cochlear box with microphone model

Once a hole has been implemented, the modelling proceeded with the insertion of the model of the microphone (mph) in the cochlea. The mph model consists basically of two walls that represent its left and right sides, and a membrane that models the behaviour of the pressure sensor. The mph width is 0.4 mm while its penetration is set to 0.2 mm . The mph model implemented in cochlear box is depicted in fig. 3.22, its detail are depicted instead in fig. 3.23, which illustrates a box section next to the RW. The walls and the membrane are implemented in the code in a different

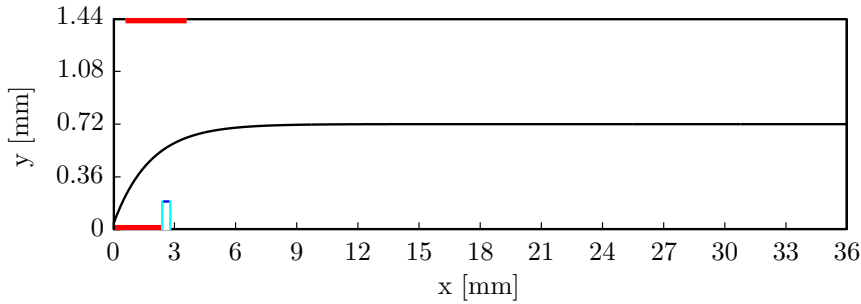


Figure 3.22: Cochlear box with mph model (cyan and blue lines).

way, as they are conceptually different structures. As a consequence, their model will be explained separately.

Walls

The implementation of the walls has been a difficult task. The immersed boundary method was used again, following the advice found in [22] and [15]. As a result the equations for the walls are assumed to have the following shape [22] :

$$\mathbf{f}(\mathbf{x}_s, t) = \alpha \int_0^t \mathbf{u}(\mathbf{x}_s, t') dt' + \beta \mathbf{u}(\mathbf{x}_s, t), \quad (3.31)$$

3.5. Configuration with the microphone

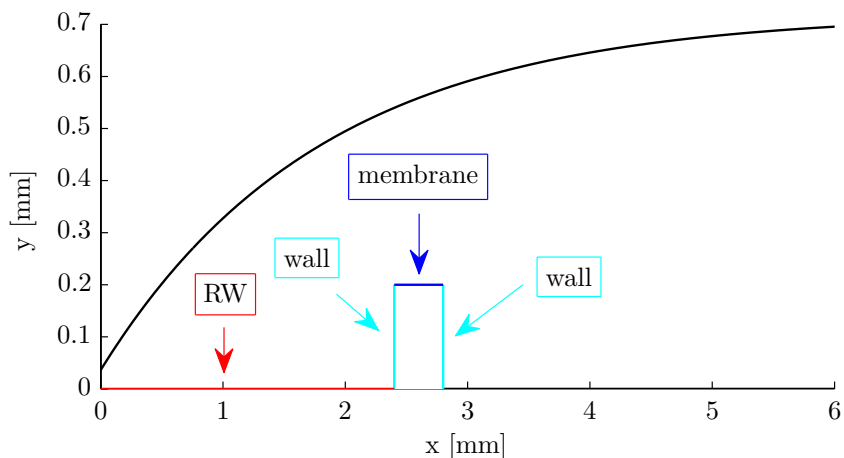


Figure 3.23: Portion of the cochlear box with mph model (cyan and blue lines).

where \mathbf{x}_s is the position of the point of the wall considered, α and β are parameter chosen case by case. As the wall is supposed to be infinitely rigid, the no-slip condition imposes that the velocity on the wall vanishes. Thus α and β should be theoretically infinite. On the other hand, high values of α and β result in instability of the simulation.

The first implementation was done using the same grid and the same δ (i.e. the parameter to pass from the Eulerian grid to the Lagrangian grid and vice-versa, see 2.3) used to implement the BM in the code. As a result the stability field was limited and the maximum values of α and β were actually low: the velocities on the wall were reduced just to one third of their values in the configuration without mph. This was pretty unsatisfying; as a consequence, in order to increase the values of α and β , first the Lagrangian grid points were increased and subsequently the δ used for the interpolation was modified.

The first resolution was already introduced in 3.3.4, the Lagrangian grid has been implemented in a way that there are two wall points per each

fluid grid cell. This solution helped to increase the values of α and β , and decreased the spikes and the discontinuities that there were present along the wall.

The change of δ increased noticeably the range of stability of the numerical method. The previous δ , defined in 3.16 and 3.17, spreads the forces over four points of the fluid grid, with a low smoothing and easier chances of instability. Therefore it was necessary to define a new δ that could spread the forces on more points. Following the instructions given in [8], the interpolation function of the wall was defined in the following way:

$$\delta = \delta_x(r_x)\delta_y(r_y) \quad (3.32)$$

$$\begin{cases} \delta_h(r_h) = \frac{1}{4\Delta_h} \left(1 + \cos \left(\frac{\pi r_h}{2\Delta_h} \right) \right), & \text{if } |r_h| \leq 2\Delta_h; \\ \delta_h(r_h) = 0, & \text{if } |r_h| > 2\Delta_h; \end{cases} \quad (3.33)$$

where

$$h = x, y;$$

r_h is the distance from the wall's point considered along the h -direction, Δ_h is the meshwidth of the Eulerian grid along the h -direction. This interpolation function involves *sixteen* fluid grid points around the wall point considered, as depicted in fig. 3.24. With this implementation of δ , the values of the velocity on the wall were reduced in the range between 5% and 10% of their value without the mph. Although these values are for certain aspects still too large, they were considerate adequate for a first approach to the study of a microphone model implemented inside a cochlear box. Further developments could improve the model of the mph even more, but they have not been implemented in this thesis.

Membrane

The implementation of the membrane on the top of the microphone was straightforward. IBM was used also for this element, the equations for the

3.5. Configuration with the microphone

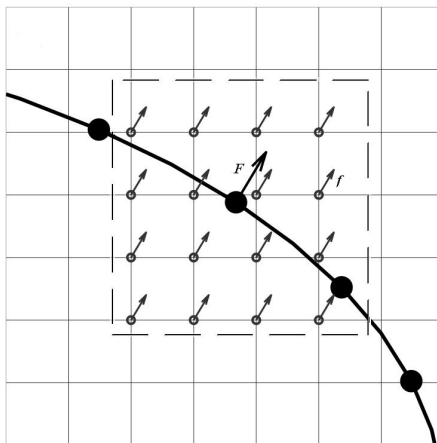


Figure 3.24: Distribution of the wall forces on the fluid grid with the new δ defined: \circ indicates the Eulerian grid, \bullet the Lagrangian one.

membrane are written in the following way:

$$\begin{aligned} f_x &= k_{m,x} \eta_{m,x}, \\ f_y &= k_{m,y} \eta_{m,y}, \end{aligned} \quad (3.34)$$

where η_m is the displacement of the membrane, k_m is the stiffness of the membrane, constant along the membrane length; the x and y subscripts indicate the direction along which the properties are considered. These relations assume again that the damping and mass of the membrane are zero, or better, dominated by the fluid. For the membrane the following first guess values were used:

$$\begin{aligned} k_{m,x} &= 2.083 \cdot 10^9 \frac{N}{m^3}, \\ k_{m,y} &= 2.083 \cdot 10^8 \frac{N}{m^3}. \end{aligned} \quad (3.35)$$

Also in this case the Lagrangian grid used to follow the movement of the membrane is implemented with two grid points per each fluid grid cell (see

3.3.4), basically to avoid the presence of small velocity discontinuities on the membrane. The interpolation function in this case is the one that interpolates on four grid points, as there were no stability problems concerning the membrane.

Chapter 4

Results

In this chapter the main results obtained in this thesis will be presented. It must be underlined again that the main part of the work has been focused in the change of cochlear box configuration, the section reserved for this topic is thus the leading part of the chapter. The configuration with the microphone, although allowing already important considerations, has to be considered just a first approach to the simulation of intra-cochlear receivers.

Before showing the results, it is first necessary to introduce the abbreviations that will be used in the follow-up of the chapter.

- *BC*: indicates the base box configuration, i.e. the box with RW on the left side and the flat membrane.
- *MRW*: indicates the box configuration with moved RW, i.e. the arrangement with flat membrane and RW at the bottom side of the box.
- *PC*: indicates the proposed box configuration, with RW at the bottom side and curved membrane; as the proposed configuration was tested in three different configurations, with different shifting of the RW, the different layouts are abbreviated as:
 - *PC1*, for the configuration with the RW's left edge at the left-lower corner of the box (i.e. case 1 in 3.3.4);

4.1. Constant OW's velocity simulations

- *PC2*, for the configuration with the RW's left edge 0.75 mm far from the left-lower corner of the box (i.e. case 2 in 3.3.4);
- *PC3*, for the configuration with the RW's left edge 1.5 mm far from the left-lower corner of the box (i.e. case 3 in 3.3.4).
- *noMPH*: indicates the PC1 with the hole for the insertion of the mph.
- *MPH*: indicates the PC1 with the microphone model implemented inside.

4.1 Constant OW's velocity simulations

Different aspects of the different configurations have been inspected. In 2.1.3 the importance of the travelling wave conveying the signal from the fluid to the basilar membrane was explained. Besides, the structure of the BM was described, and this implies a different distribution of the displacements on the BM and the shifting of the characteristic point (whose collocation gives information on the frequency of the signal) when varying the frequency of stimulation of the OW. For this reason, the distribution of the displacements on the BM will be addressed more thoroughly. In addition, the velocity and the pressure field of the fluid will be displayed, in particular the characteristics of the latter will be examined with more interest as it leads to important conclusions.

4.1.1 BM's displacement

It is interesting to start displaying the instantaneous position of the BM. Fig. 4.1 shows the instantaneous positions of the BM's points along y (i.e. the direction locally normal to the membrane as the membrane is flat) in the BC with a stimulation of the OW of $f = 1\text{ kHz}$; fig. 4.2 illustrates the same plot but this time for the MRW and fig. 4.3 for the PC1, but as the direction locally normal to the BM is not the y -direction, the displacement is plotted along n (see 3.3.4). The three figures have been cut at half length

of the cochlea, as in the second half the displacements vanish and thus there is no interesting information to extract.

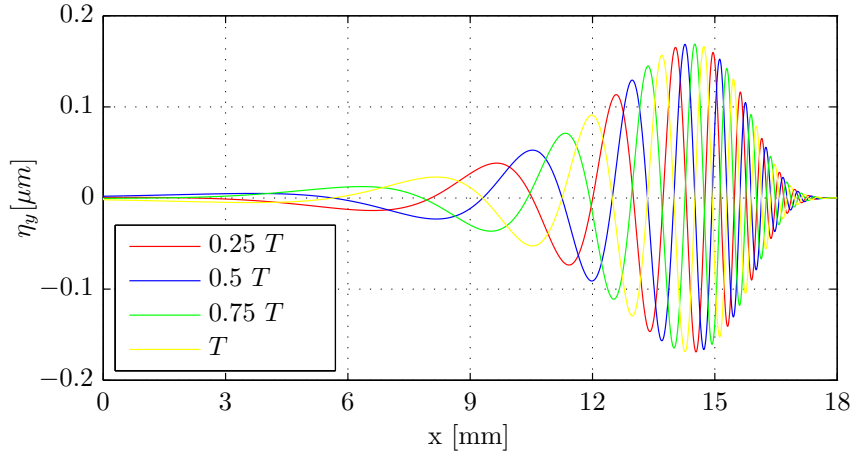


Figure 4.1: Instantaneous BM motion along y with BC at four different timesteps, $f = 1kHz$.

T is the period of oscillation of the OW, the timestep for the representation of the curves is $\frac{T}{4}$. When the BM's motion is described, two different kinds of movement can be highlighted. One is an oscillatory movement progressing in x , i.e. the *travelling wave*, which has been introduced in 2.1.3, and it is noticeable in all the three figures as the peaks in the curves moving forward. The second is a wave that does not move along x , i.e. a *standing wave*, which consists of an oscillatory movement in y ; this component of the motion is not clearly noticeable in the figures presented.

There are no evident differences in the behaviour of the BM in the three cases, except for the amplitude of the displacement. While for BC and MRW the BM experiences movements of the same amplitude, in the PC1 the BM experiences displacements one order of magnitude lower than those in the BC. This is not a good characteristic of the PC1. Although it is not demonstrated that the signal sent to the brain through the IHC

4.1. Constant OW's velocity simulations

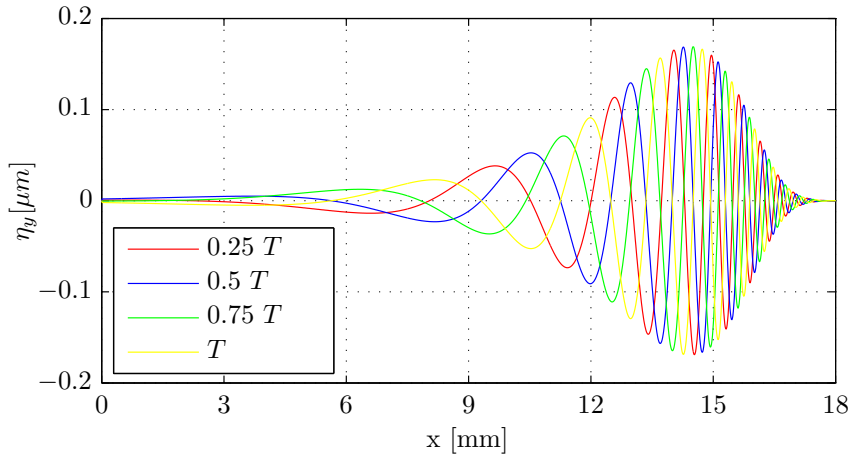


Figure 4.2: Instantaneous BM motion along y with MRW at four different timesteps, $f = 1\text{kHz}$.

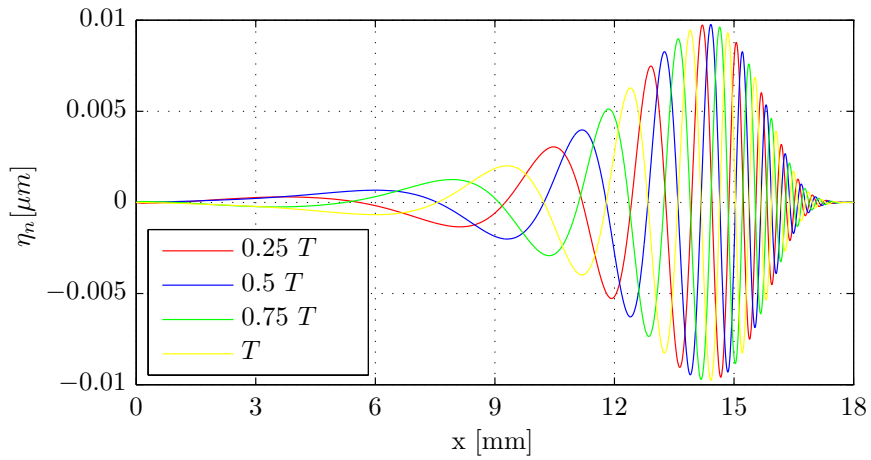


Figure 4.3: Instantaneous BM motion along n with PC1 at four different timesteps, $f = 1\text{kHz}$.

is directly related to the amplitude of the displacement, it is clear that a lower displacement of the BM results in a reduced movement of the cochlear partition; thus it is reasonable to think that there is some kind of relation between the amplitude of the BM's displacement and the output signal sent to the brain. Some physical reasons to explain this kind of behaviour of the PC1 will be given in the section of this chapter concerning the velocity field of the PC1.

The three plots shown, concern the BM's movement with a $1kHz$ stimulation; when the frequencies are increased the behaviour changes radically. Fig. 4.4, 4.5 and 4.6 illustrate the same plots but with a $4kHz$ stimulation of the OW. The x -axis in the figures has been cut at $12mm$, as the

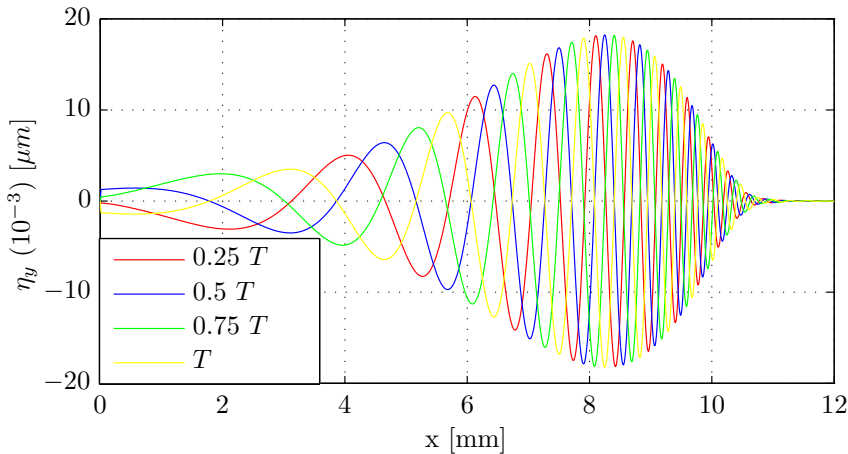


Figure 4.4: Instantaneous BM motion along the y -direction with BC at four different timesteps, $f = 4kHz$.

information stays just in this part of the cochlear box. As expected, the characteristic point (i.e. the point in which the BM reaches its maximum displacement at a given frequency) moves leftwards with increasing frequencies in the models presented. As a matter of fact in this configuration the *apex* of the BM would be placed at the right side of the BM; as a con-

4.1. Constant OW's velocity simulations

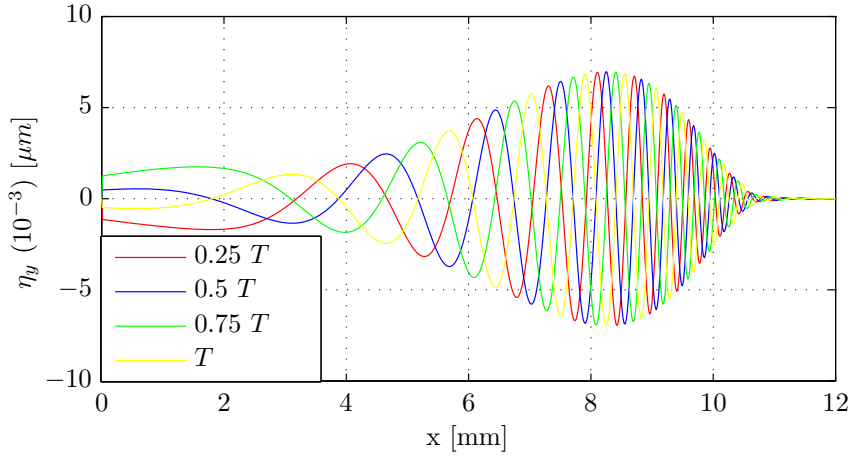


Figure 4.5: Instantaneous BM motion along the y -direction with MRW at four different timesteps, $f = 4\text{kHz}$.

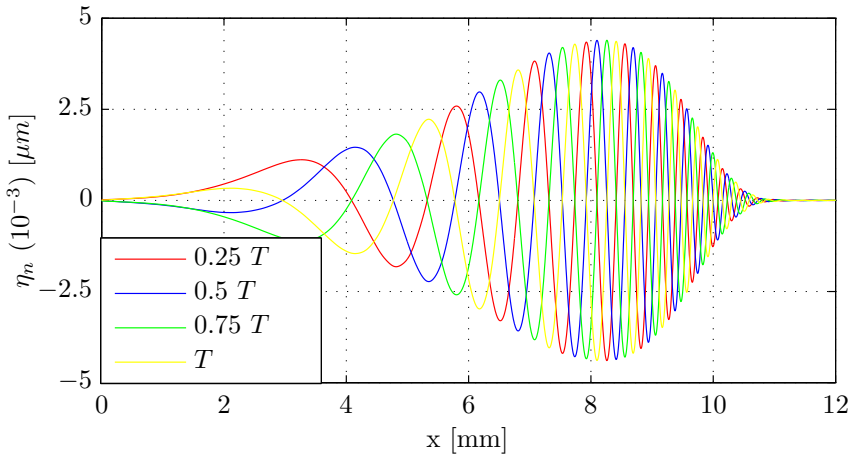


Figure 4.6: Instantaneous BM motion along n with PC1 at four different timesteps, $f = 4\text{kHz}$.

sequence from fig. 2.7 it can be seen that the characteristic point in the model presented must move leftwards with increasing frequencies.

With a 4 kHz stimulation, the magnitudes of the displacements are different for each of the three configurations, and the BM's displacements in the PC1 have the same order of magnitude of the other two configurations.

At this frequency we can see remarkably well the standing wave in the MRW configuration (fig. 4.5) in the left side of the BM. This wave is supported by the nearly symmetrical configuration of the box. To investigate this aspect a box configuration where the OW and the RW have the same size and they are placed at the same x-position respectively at the top and at the bottom side of the box was tested. When low frequencies of stimulation were run, the differences between BC, MRW and this configuration were really unnoticeable. But when the frequencies are increased, the CP moves leftwards and the RW position effect is more important on fluid dynamics. As a result, in the completely symmetric configuration the travelling wave almost disappears with frequencies in the range $4 \div 5 kHz$; the fluid in this case just moves from the OW to the RW without generating any travelling wave, exclusively a standing wave. MRW configuration is almost symmetric, the travelling wave loses significantly its strength with higher frequencies, and this is demonstrated by the large difference between the magnitude of the displacement of the CP in the BC and the one in the MRW.

In fact, also in fig. 4.4 a standing wave can be noted in the first part of BM's length. This is due to the BM's shape, the flat membrane at high frequencies yields a standing wave and a reduction in strength of the travelling wave (see also fig. 4.10 which clearly presents this aspect). The explanation for this behaviour can be found in the velocity field, this conformation of the BM promotes the effect introduced above, i.e. when the frequency becomes higher an increasing portion of the fluid moves in the cochlea directly from the OW to the RW without generating a travelling wave.

The PC1 does not exhibit this behaviour, as its BM's shape is not flat and gives to the overall configuration an high rate of asymmetry. Looking at the BM's displacements from another point of view, it can be seen that

4.1. Constant OW's velocity simulations

this is a favorable feature of the new configuration. Figs. 4.7, 4.8 and 4.9 illustrate the envelope of BM displacements at three different frequencies along BM's normal direction for the three configurations.

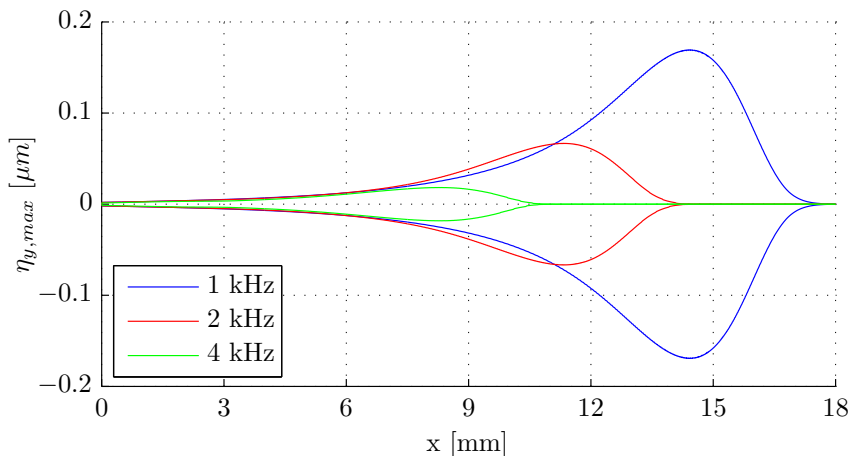


Figure 4.7: Envelope of BM displacements along the y -direction with BC at the three frequencies tested.

In the configurations with the flat membrane the envelope of the displacements at 1 kHz includes almost entirely the envelopes at higher frequency; this is not a good characteristic. The simulations are run with a constant signal coming from the OW (the velocity of the stapes is kept constant through all these simulations, see 3.3). As a result it is reasonable to think that each point of the BM reaches its maximum displacement when it is the characteristic place of a given frequency, in this way the elements in the cochlea partition can effectively determine if the particular point is the CP or not. Fig. 4.7 and fig. 4.8 do not show the behaviour expected. On the contrary fig. 4.9, which concerns the displacements envelope in the PC1, illustrates that each point experiments its maximum displacement when it is the CP of a given frequency. Consequently, although the amplitude of the displacement is much lower at low frequencies, the overall

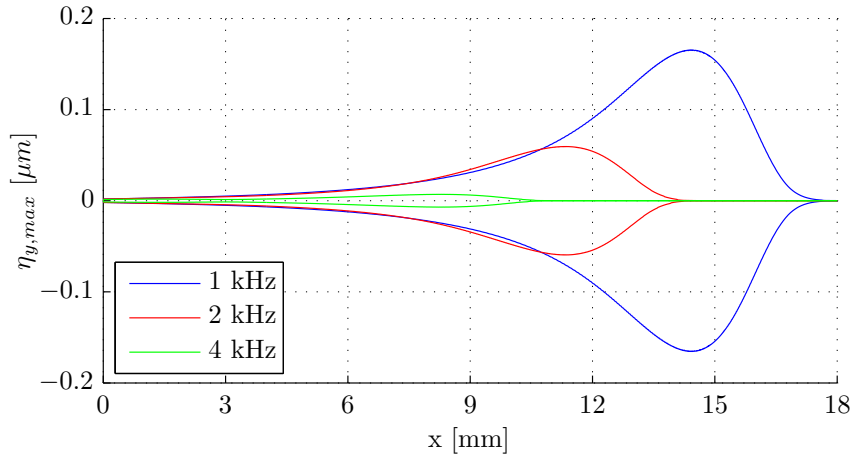


Figure 4.8: Envelope of BM displacements along y with MRW at the three frequencies tested.

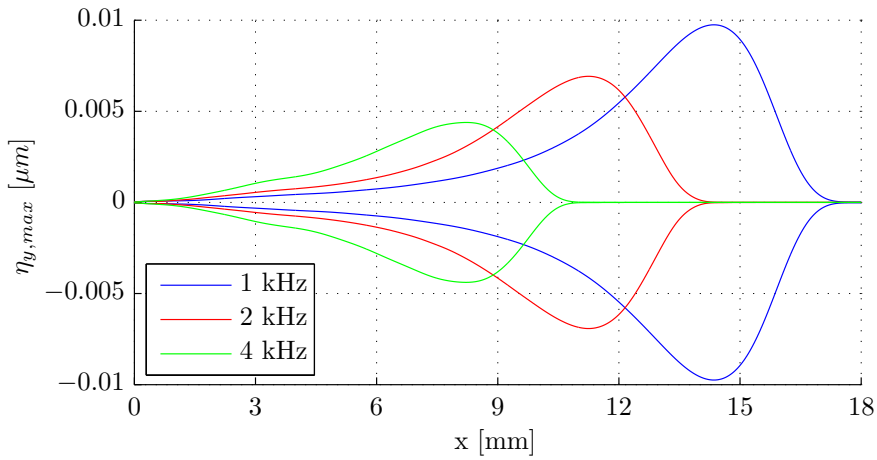


Figure 4.9: Envelope of BM displacements along n with PC1 at the three frequencies tested.

4.1. Constant OW's velocity simulations

behaviour of the PC on the spectrum is more favorable.

Finally fig. 4.10 illustrates the value of the CP's displacement along the direction perpendicular to the BM in that point, for each frequency and configuration tested with the same OW's velocity magnitude.

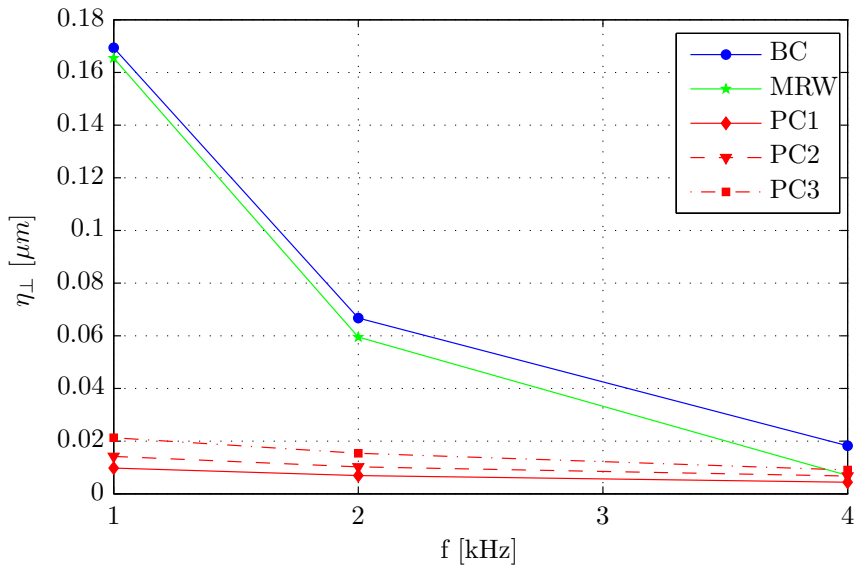


Figure 4.10: CP displacement for each configuration and frequency tested.

The figure underlines an important property of the PC, the shifting of the RW produces an amplification of the displacements with all the frequencies tested. Additional simulations have been run shifting the RW in the MRW. In these simulations, the effect of the alteration of the RW position was an increase of the BM displacements for some cases, a reduction for others, depending on both frequency and distance between the lower left corner and the left edge of the RW.

The influence of the RW position has not been investigated in details, although it is important to underline this feature. The location of the RW chosen in the definitive configuration (PC1) is completely arbitrary, as it

was not possible to define some parameters to determine a location of the RW that could better model the position of the RW in a real human cochlea.

4.1.2 Velocity field

To display the velocity field the mean on a period of the velocity magnitude will be used. The first plots that are presented concern the velocity field of BC (fig. 4.11), MRW (fig. 4.12) and PC1 (fig. 4.13) with a 1 kHz stimulation of the OW. Again, as the velocity magnitude is zero in all the second half length of the cochlea, just the first half of cochlear box length is displayed.

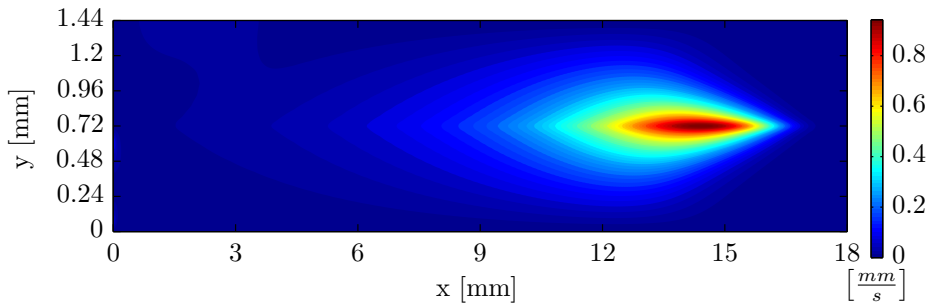


Figure 4.11: Mean over a period of the velocity magnitude ($|\bar{u}|$) in the BC at 1 kHz .

It can be seen that there are no differences between BC and MRW at 1 kHz , as expected from the results on BM's displacements presented previously. On the contrary the plot is radically different for the PC1, the illustration explains why the signal is lower in the PC1 configuration.

It must be noticed that the mean velocity on the membrane is almost zero on the period. It is interesting to show a vector plot on a sector placed in the lower-left corner of the cochlea. In order to highlight the characteristics of this flux, four snapshots (fig. 4.14 to 4.17) in the period have been plotted. Together with the vector field, the velocity magnitude field is also shown.

4.1. Constant OW's velocity simulations

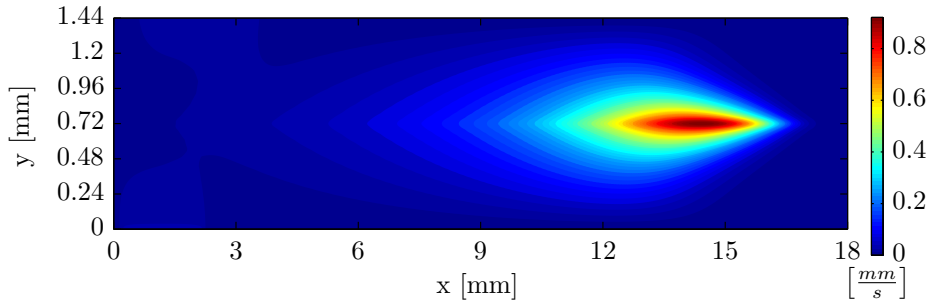


Figure 4.12: Mean over a period of the velocity magnitude ($|\bar{u}|$) in the MRW at 1 kHz.

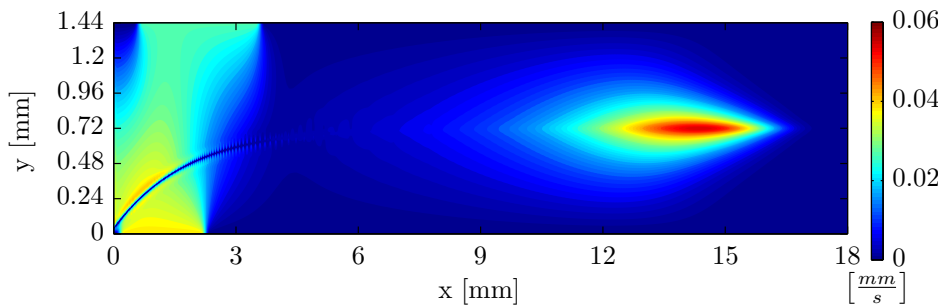


Figure 4.13: Mean over a period of the velocity magnitude ($|\bar{u}|$) in the PC1 at 1 kHz.

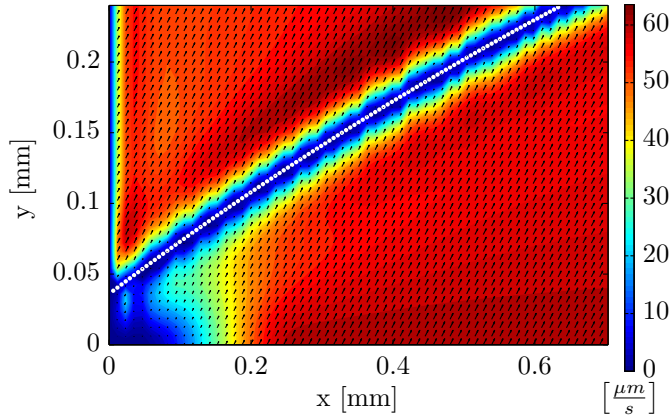


Figure 4.14: Vector plot and velocity magnitude field of a sector of the cochlea at $t = 0.25T$ with PC1, the white dots indicate BM's points.

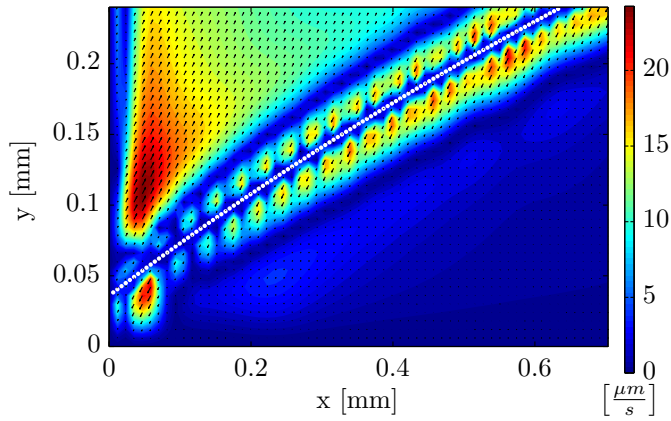


Figure 4.15: Vector plot and velocity magnitude field of a sector of the cochlea at $t = 0.5T$ with PC1, the white dots indicate BM's points.

4.1. Constant OW's velocity simulations

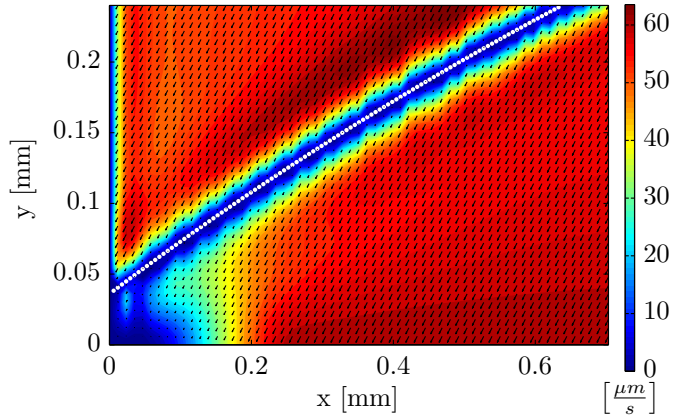


Figure 4.16: Vector plot and velocity magnitude field of a sector of the cochlea at $t = 0.75T$ with PC1, the white dots indicate BM's points.

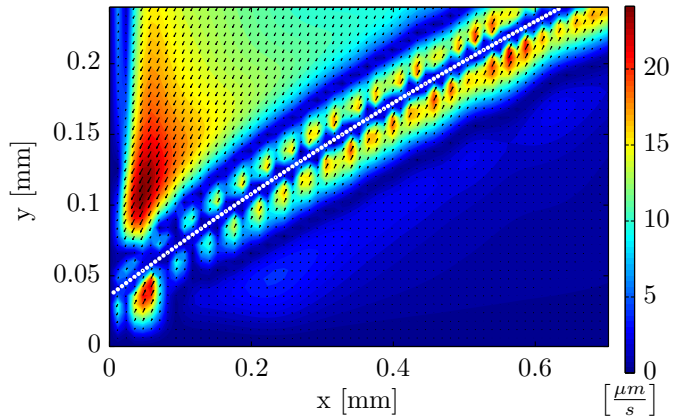


Figure 4.17: Vector plot and velocity magnitude field of a sector of the cochlea at $t = T$ with PC1, the white dots indicate BM's points.

It can be noticed that the velocity is almost always tangential to the membrane, both when the OW or the RW is pushing on the fluid. This is due to the BM's geometry that, as a result of the new conformation, in the scala tympani is more "streamlined" with the flux and thus less stimulated by the fluid. Conversely in the scala vestibuli the particular geometry creates recirculation zones which result in almost tangential fluid in the upper part of the BM. Thus in the PC the fluid does not impact directly on the BM but almost flows along its surface; this is the reason for the overall reduction of BM's displacements with respect to BC and MRW noticed previously.

It was noticed in fig. 4.10 that the configurations with the flat membrane experience a big reduction of the displacement when the frequency of stimulation is increased. It was stated that this feature was due to the fact that at high frequencies a big fraction of the fluid moves directly from the OW to the RW, and, as a consequence, it generates a standing wave and the strength of the travelling wave decreases. This fact is well illustrated in fig. 4.18, that shows the magnitude of the mean velocity field in MRW for a 4 kHz stimulation of the OW.

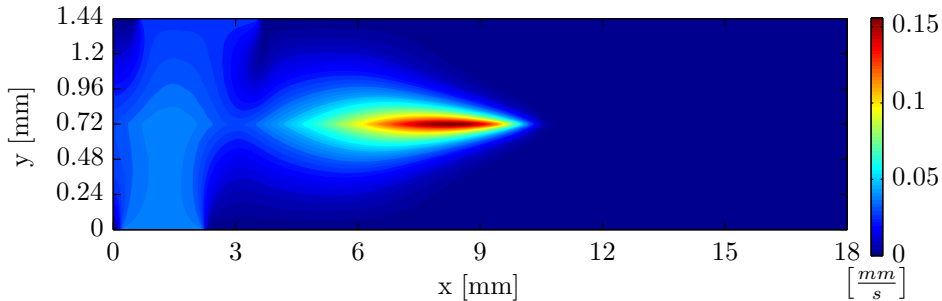


Figure 4.18: Mean over a period of the velocity magnitude ($|\bar{u}|$) in the MRW at 4 kHz .

In the figure can be seen that the peak of the velocity has decreased of almost one order of magnitude compared to the case of fig. 4.12. Moreover in this figure the trace of flux directly going from the OW to the RW can

4.1. Constant OW's velocity simulations

be observed; this is the cause of the reduction of BM's displacements.

Finally, it was also highlighted in fig. 4.10 that a shifting of the RW in PC resulted in an increased displacement distribution of the BM. In fig. 4.19 the picture of the magnitude of the mean velocity field for the PC3 is displayed.

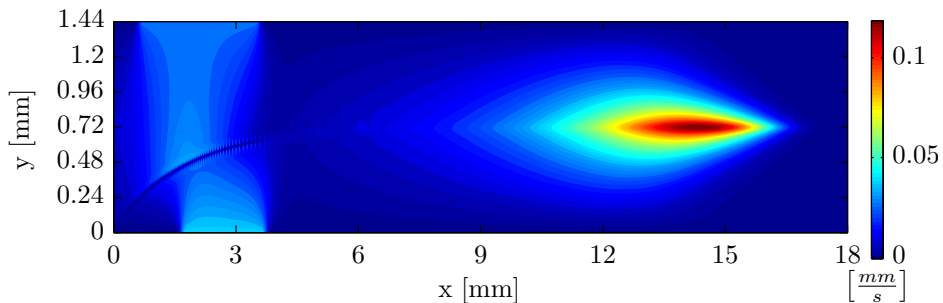


Figure 4.19: Mean over a period of the velocity magnitude ($|\bar{u}|$) in the PC3 at 1 kHz.

The figure illustrates that this configuration, compared to fig. 4.13, has a peak in velocity double compared to the PC1. This confirms the results found in the section concerning the BM's displacements. The geometry of the PC3 originate a flux inside the cochlea that stimulates better the BM, as it can be ascertained from the figure.

4.1.3 Pressure field

The pressure field allows important considerations for the purpose of this thesis. To look at the pressure results a different approach from the one utilized to treat the velocity field will be adopted. In place of the mean field, in this section the *maximum oscillation field*, which gives interesting information to collocate the microphone, will be focused on. The maximum pressure oscillation field is the field which illustrates the maximum pressure value that each point reaches over its mean pressure value. As the signal is periodic, the value of the maximum pressure oscillation is equal to the value

of the minimum pressure oscillation. The reason for which it is important to look at this field resides in the fact that this is the signal measured by the microphone. The mean pressure field results only in a bending on the mph's membrane. As a consequence, it is important to compute the mean pressure field only to control this bending that, if too big, can result in a reduction of accuracy. Presently, it is important to look at the signal that a microphone would measure in each point of the cochlea.

When treating the pressure in the cochlea, it is important to define a point whose pressure is used as a reference value. The microphone that will be inserted in the cochlea measures the relative pressure and the reference value is the pressure in the eustachian tube (see fig. 2.1) [18]. The pressure in the eustachian tube must be the same pressure of the RW, as the RW's stiffness is assumed to be zero (see 3.1.1). As a consequence, in order to reproduce the signal measured by the microphone, the reference value for the pressure reference is placed in the center point of the RW in the figures that will be shown below.

The maximum pressure oscillation field resulting from a 1 kHz stimulation of the OW, for BC, MRW, PC1 and PC3 is shown, respectively, in fig. 4.20, fig. 4.21, fig. 4.22 and fig. 4.23. Again, the plots show only half length of the cochlea, as in the other half the pressure signal is constant everywhere.

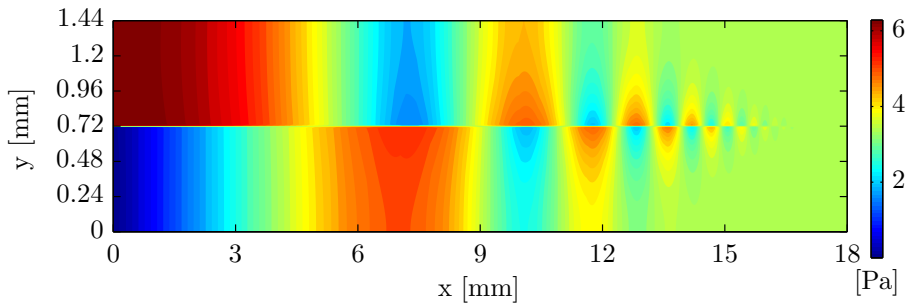


Figure 4.20: Maximum pressure oscillation field in the BC at 1 kHz .

It can be observed that all the plots give an important information: no

4.1. Constant OW's velocity simulations

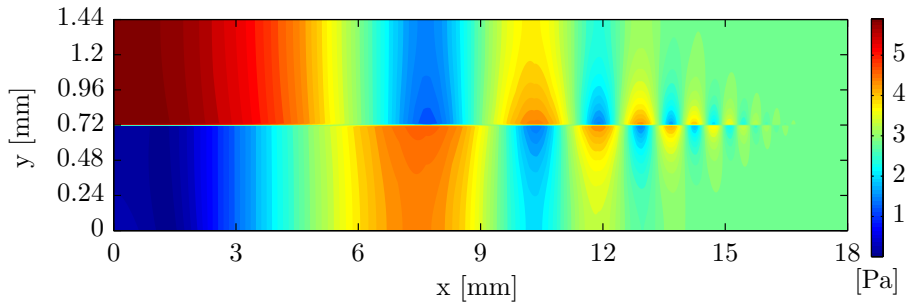


Figure 4.21: Maximum pressure oscillation field in the MRW at 1 kHz.

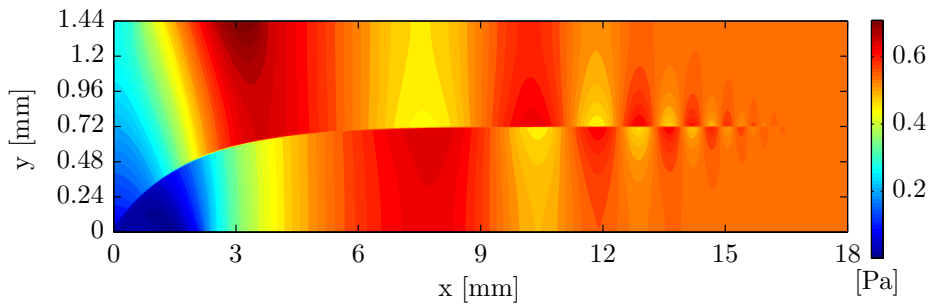


Figure 4.22: Maximum pressure oscillation field in the PC1 at 1 kHz.

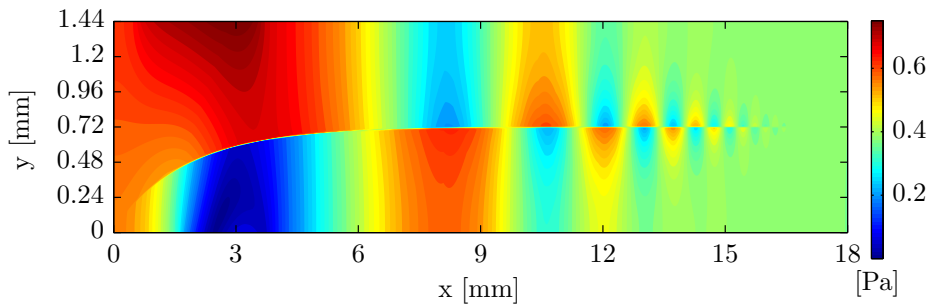


Figure 4.23: Maximum pressure oscillation field in the PC3 at 1 kHz.

matter where the RW is placed, the pressure signal above it is weak. From a practical point of view, the most accessible place for the surgery is the RW; as the microphone in that place would not receive any message, it is necessary to locate it in another position. From the figures it can be also noticed that the further away the mph is placed from the RW, the louder it is the signal received. The final location of the mph matches the two factors, therefore in this work its effects are tested when it is implemented next to the RW.

Further considerations on the pressure field will be done in the next section, where the pressure field will be used to make a comparison with the experimental results.

4.2 Comparison with experimental data

The procedure to achieve this comparison has been explained in 3.4. On the other hand, before showing the results obtained, it is necessary to make some considerations now that the pressure field of the cochlea has been presented. The experimental data obtained by Nakajima et al. [17] are expressed in dB , whose definition is:

$$p [dB] = 20 \log_{10} \left(\frac{p}{p_0} \right); \quad (4.1)$$

it has been explained that in [17], p_0 has been set to $1Pa$, which is the pressure that has been imposed at the eardrum in their experiment. As a consequence, also the pressure fields that are presented in this section will be displayed in dB with $p_0 = 1 Pa$. Moreover, the pressure computed in [17] is the maximum pressure oscillation, thus again the maximum pressure oscillation field, will be shown.

This section is structured into two parts: the first part concerns the comparison of the results from the MRW, the second deals with the comparison of the results coming from PC1.

4.2. Comparison with experimental data

4.2.1 Comparison with the results from the MRW

It is useful to look at the measurement points of fig. 3.19 in the maximum pressure oscillation field for this configuration. Fig. 4.24 illustrates this with frequency of OW oscillation of 1 kHz . Again, the field is shown just in the first half of length of the cochlea. In the figure, there are two black lines, which indicate the position of the OW and the RW.

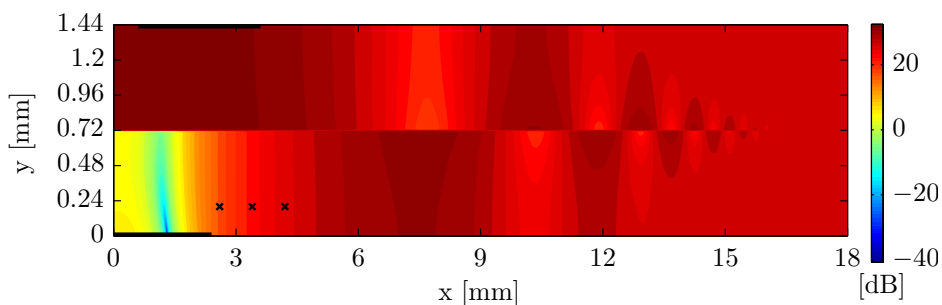


Figure 4.24: Maximum pressure oscillation field and measurement points with MRW at 1 kHz .

In fig. 4.25 a portion of the maximum oscillation field has been plotted, to show more accurately the pressure properties in the neighborhood of the RW. Moreover, the figure shows the acronyms used to address each of the three measurement stations., i.e. ST1 ("ST" stand for scala tympani) for the first point from the left, ST2 for the second and ST3 for the third one.

Computing the values found in these points, then changing the frequencies (four oscillation frequencies were simulated: 500 Hz , 1 , 2 and 4 kHz ; see 3.4) and repeating the same procedure for each of them, the values to be compared with the experimental data can be determined. The results of this procedure are plotted in fig. 4.26. Together with the measures of ST1, ST2 and ST3 at the different frequencies, three additional curves that are used to describe the experimental results are depicted, and they are the reproduction of the blue curves of fig. 3.15. As a consequence, the dashed lines indicate the lower and upper limit of the experimental data, whereas

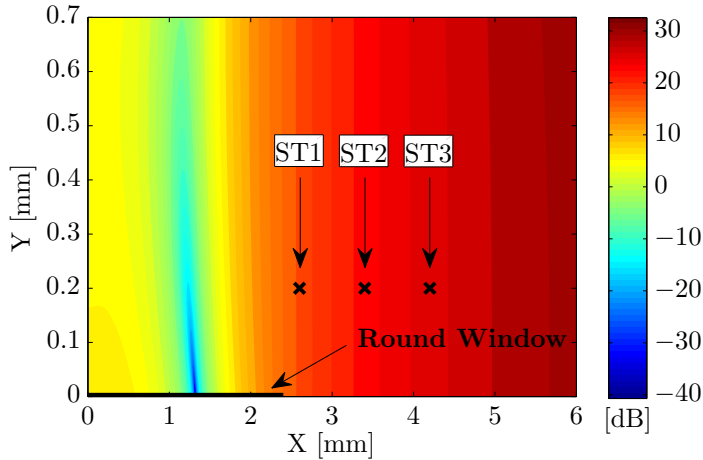


Figure 4.25: Maximum pressure oscillation field and measurement points with MRW in the vicinity of the RW at 1 kHz .

the solid line reproduce the mean value of the experimental data.

It can be noted that the curves of the experimental data and the ones of the numerical results do not match. Moreover their trend is extremely different. This comparison is thus not satisfactory, and this stems from the region in the vicinity of the RW which is not simulated properly.

4.2.2 Comparison with the results from the PC

Following the same pattern followed to show the results with MRW, the maximum pressure oscillation field for the the PC at 1 kHz is first illustrated in fig. 4.27, the black crosses (X) indicate the measurement points used for the comparison. A portion of it is then shown in fig. 4.28, to highlight the field in the vicinity of the RW. Again a name is assigned to each of the three positions chosen for the comparison, the latter mentioned figure indicates the name of each point.

Finally, fig. 4.29 reports the comparison between the experimental data

4.2. Comparison with experimental data

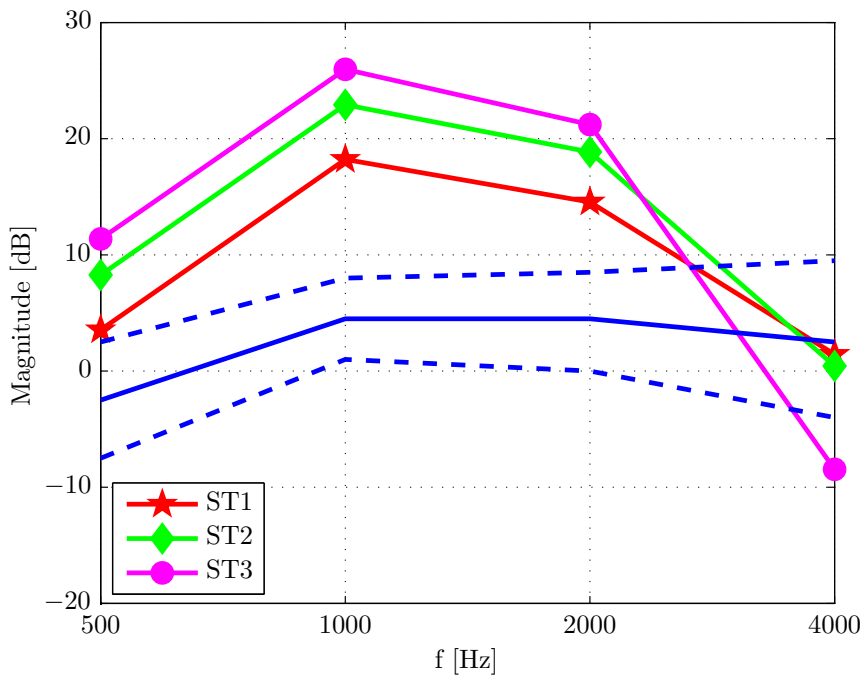


Figure 4.26: Comparison of MRW results with experimental data, which lie in the dashed blue lines whereas the solid blue line indicates their mean value.

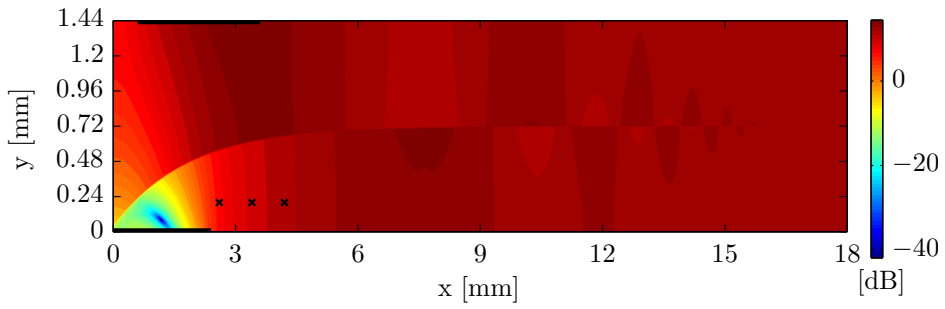


Figure 4.27: Maximum pressure oscillation field and measurement points with PC1 at 1 kHz .

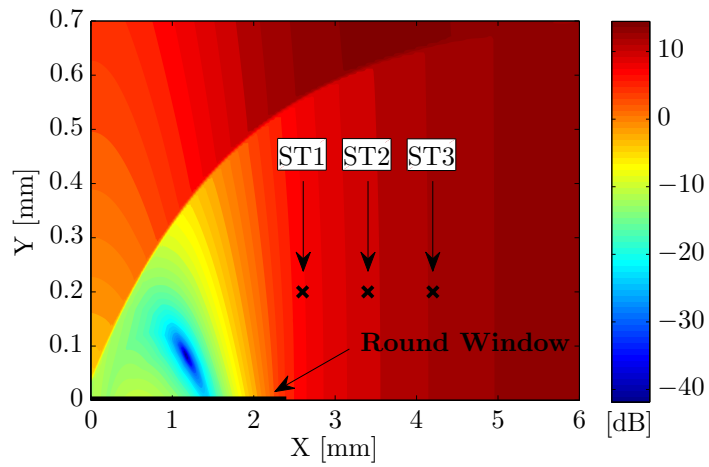


Figure 4.28: Maximum pressure oscillation field and measurement points with PC1 in the vicinity of the RW at 1 kHz .

4.2. Comparison with experimental data

and results from PC1.

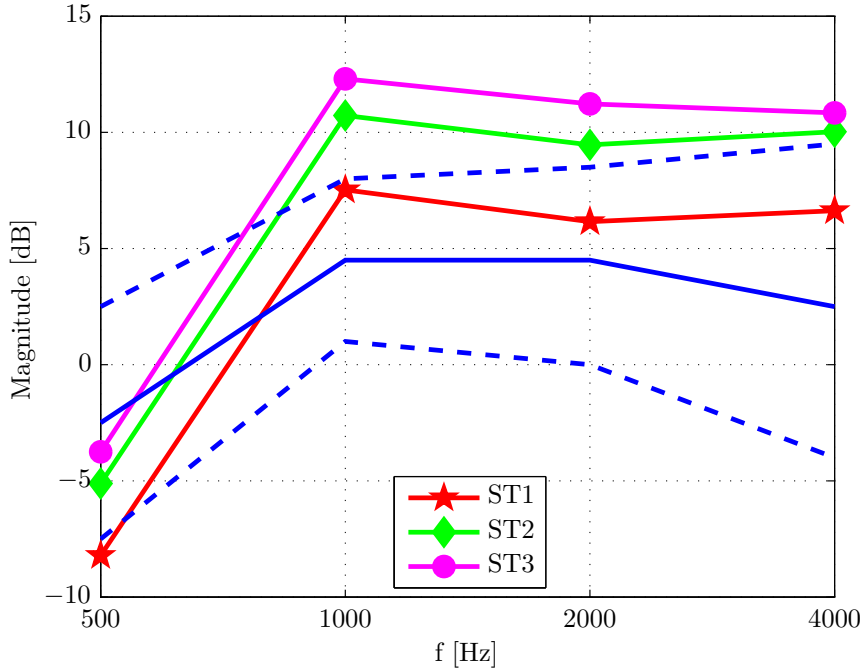


Figure 4.29: Comparison of PC1 results with experimental data, which lie in the dashed blue lines whereas the solid blue line indicates their mean value.

In this case, the experimental measurements and the numerical results show a better agreement as compared to the previous case (fig. 4.26). The pressure magnitude in *ST1* fits perfectly within the stripe of experimental values. *ST2* and *ST3*, though partly out and partly in, do not show a completely different frequency trend as previously. This comparison is considered acceptable. As a consequence, PC1 is proposed as the new cochlear box configuration to implement the intracochlear receiver.

4.3 Implementation of the microphone

As already stated in the beginning of this chapter, this part of the work has to be intended as a first approach to the implementation of the intracochlear receiver (microphone) inside the cochlea.

This part of the thesis has been structured in the same way as 4.1; thus the behaviour of the BM will be discussed first, followed by the velocity field and concluding with the pressure field.

4.3.1 BM's displacement

The values of the OW velocity set in these simulations are different from those used for the considerations in 4.1. It is thus necessary to see the results also for the case PC1, i.e. without the microphone model, to make effective comparisons between the two cases. The first plot that are shown concern the instantaneous BM's displacements, which are presented in the same way from figures 4.1 to 4.6. Thus, in fig. 4.30 and fig. 4.31 the instantaneous shape of the BM at four different timesteps respectively for the PC1 and MPH are illustrated.

The plots show that the BM behaves in the same way in the two configurations tested: there is no standing wave, and the characteristic point is in the same point. The only difference lies in the amplitude of the BM's displacement, which is reduced in the case with MPH. This feature is better illustrated by an envelope of the maximum displacement experienced by each point of the membrane. Thus, in fig. 4.32 the envelope of the BM's displacements for PC1 and MPH is shown.

The decrease of the BM at the characteristic point, passing from PC1 to MPH, is around 30%. The reasons for this reduction will be examined closely when inspecting the velocity field. There are no other differences other than the decrease of the amplitude; the dynamics of the BM is not changed by insertion of the mph. As a consequence, from the BM's membrane point of view, the configuration with the intracochlear receiver seems feasible at $1kHz$.

4.3. Implementation of the microphone

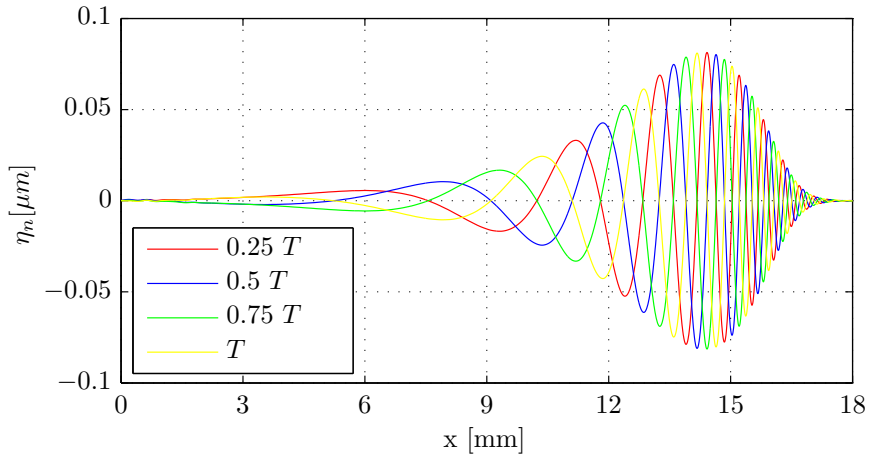


Figure 4.30: Instantaneous BM motion along n with PC1 at four different timesteps, $f = 1kHz$.

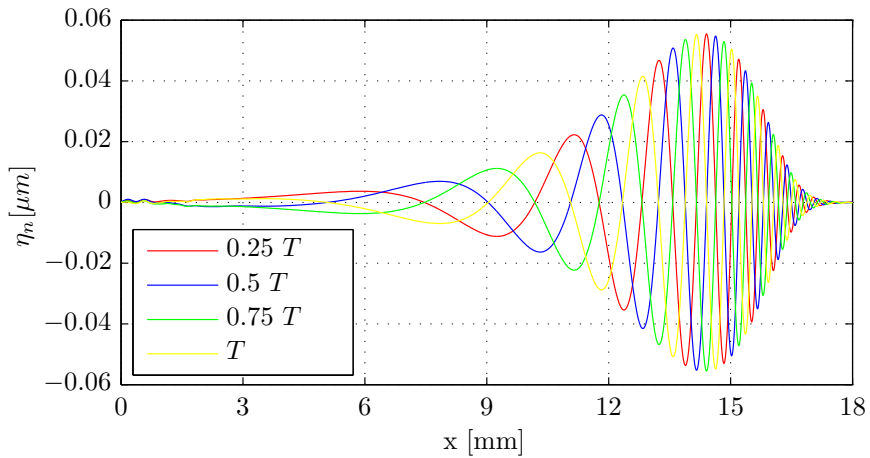


Figure 4.31: Instantaneous BM motion along n with MPH at four different timesteps, $f = 1kHz$.

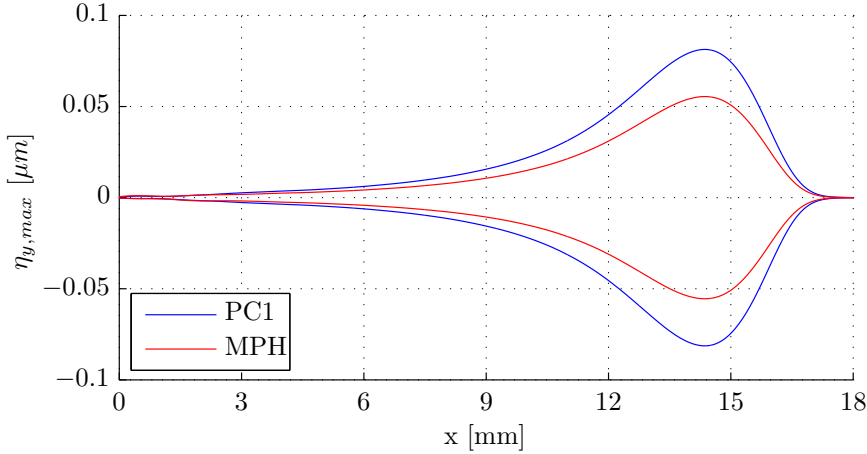


Figure 4.32: Envelope of BM's displacements along n for PC1 and MPH.

4.3.2 Velocity field

The properties of the velocity field are inspected through the mean velocity field. Fig. 4.33 and 4.34 presents the mean velocity field in the first half of the cochlear length, respectively in PC1 and MPH.

From a comparison between fig. 4.33 and 4.34 it can be noted that the velocity peaks are the same. However, in the MPH configurations these peaks are not reached on the BM at the characteristic point, but rather in the region of the mph. This results in a reduction of the overall BM's displacement, as it has been seen in 4.32.

As the critical part is in the region of the microphone, fig. 4.35 shows a sector of fig. 4.34 centred on the microphone.

At the top edge of the walls the particular geometry creates vortices, and the velocity in that region increases. It must be noticed that the presence of the mph membrane creates further agitation in that region.

4.3. Implementation of the microphone

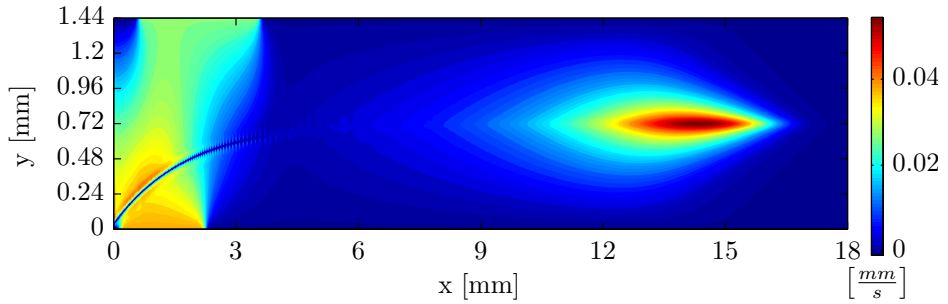


Figure 4.33: Mean over a period of the velocity magnitude ($|\bar{u}|$) in the PC1 at 1 kHz.

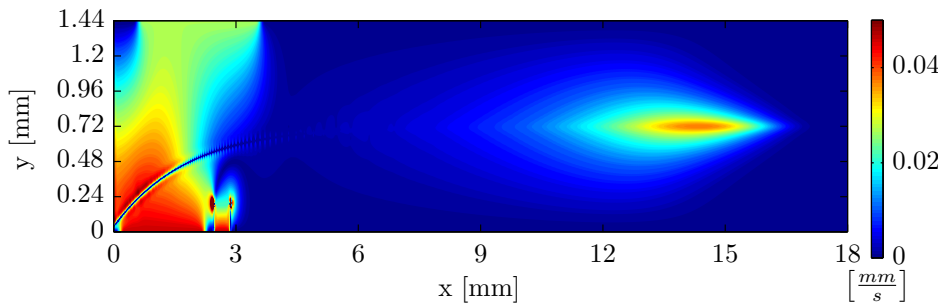


Figure 4.34: Mean over a period of the velocity magnitude ($|\bar{u}|$) in the MPH at 1 kHz.

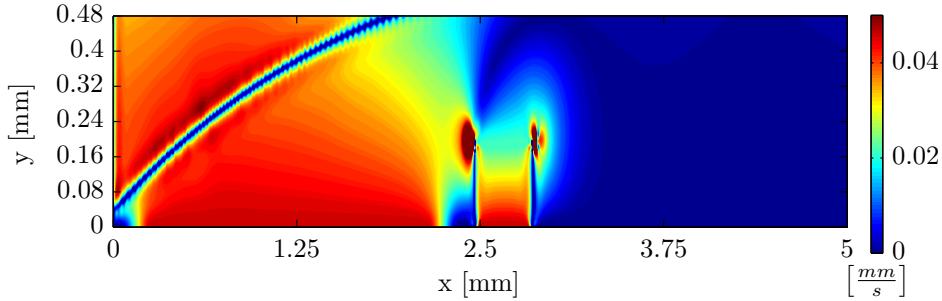


Figure 4.35: Sector next to the microphone model of the mean over a period of the velocity magnitude ($|\bar{u}|$) in the MPH at 1 kHz .

4.3.3 Pressure field

Finally, the pressure field resulting from this configuration will be discussed. In figures 4.36 and 4.37 the maximum oscillation pressure field at 1 kHz with, respectively, the PC1 and the MPH, are displayed.

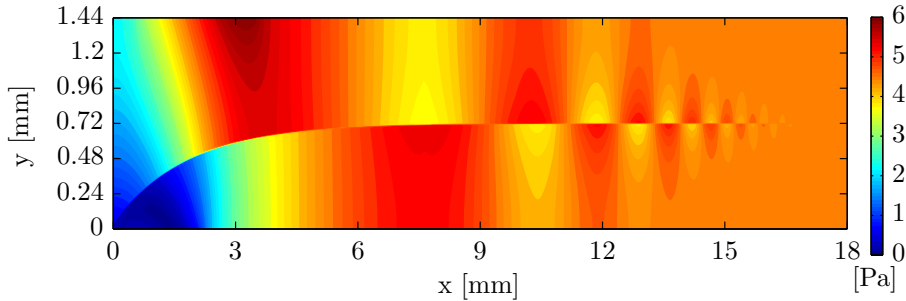


Figure 4.36: Maximum pressure oscillation field in the PC1 at 1 kHz .

In the region inside the microphone there are pressure oscillations of high intensity. This is considered to be a numerical error, but for time constraints the effect has not been studied further. Its resolution is proposed as future work to develop the simulation of intracochlear receivers. The results shown

4.3. Implementation of the microphone

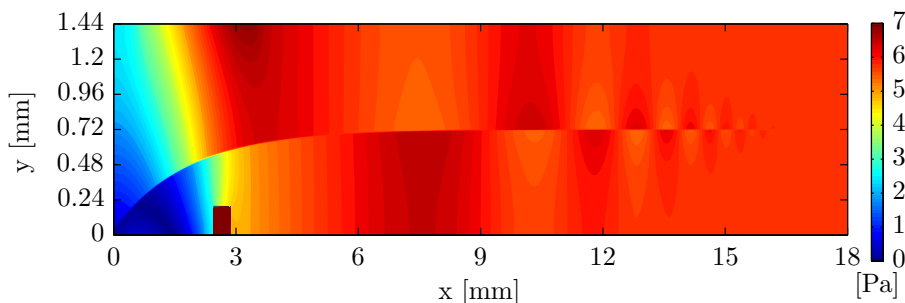


Figure 4.37: Maximum pressure oscillation field in the MPH at 1 kHz .

obscure that part. As it is now, this does not seem a physically meaningful solution for the fluid inside the microphone.

From a comparison between the two pictures, it can be concluded that, except for an increase of the pressure values of about $0.7 \div 1\text{ Pa}$, and an action of the mph that changes locally the field, the overall pressure field is not affected by the presence of the mph. Both the pressure and velocity field suggest that at 1 kHz the insertion of the microphone in that position is feasible and the signal transmitted to the BM is the same as the one transmitted without the microphone, although slightly decreased in amplitude. After all, the section dealing with BM displacements already indicated this conclusion.

This result encourages the development of the new configuration proposed for the cochlear implants, at least from the cochlear point of view. The signal at the microphone has to be verified, to see if its intensity is reasonably high. As a consequence, in the following of this chapter the signal on the membrane of the microphone, will be analyzed.

4.3.4 Dynamic of mph's membrane

The membrane represents the sensor of the microphone and its behaviour is modelled through eq. 3.34. From this equation it can be noticed that the forces exerted on the membrane, which are directly related to the

input signal of the microphone, are uniquely determined by mph's membrane displacements. As a consequence, to understand the features of the signal gathered by the microphone, it is important to show the behaviour of these displacements during one period of stimulation. Fig. 4.38 and 4.39 illustrate the displacements of the membrane respectively along x and y . x_{memb} is an axis parallel to the x -direction, with its origin on the left edge of the membrane.

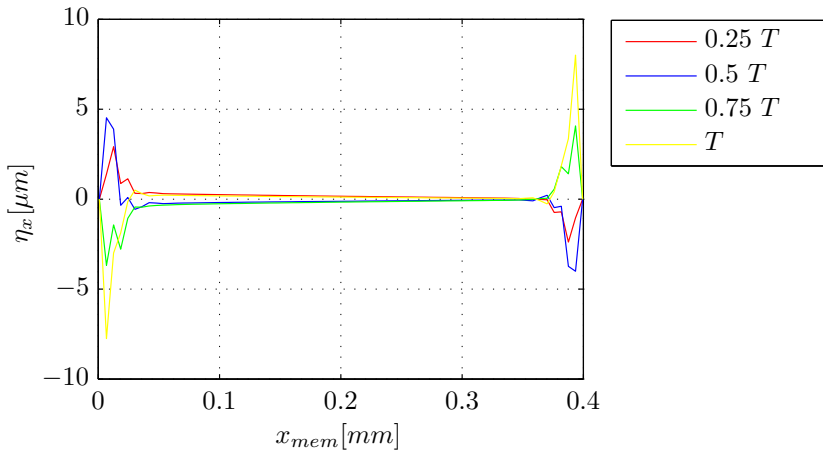


Figure 4.38: Displacements along the x -direction of the mph membrane at four different timesteps.

It can be seen from the figures that the displacements along the x -direction are negligible in the middle of the membrane, while they are not at the left and the right edges of it. Thus the vortices that can be observed in fig. 4.34 result in a strain of the mph's membrane. The displacements along y are not affected by the vortices at the boundaries. In the middle of the membrane the displacements are constant both along x and y .

The most important feature to be inspected for the purposes of this work is the force that the fluid exerts on the membrane that, as previously said, can be computed easily once that the displacements are known. The

4.3. Implementation of the microphone

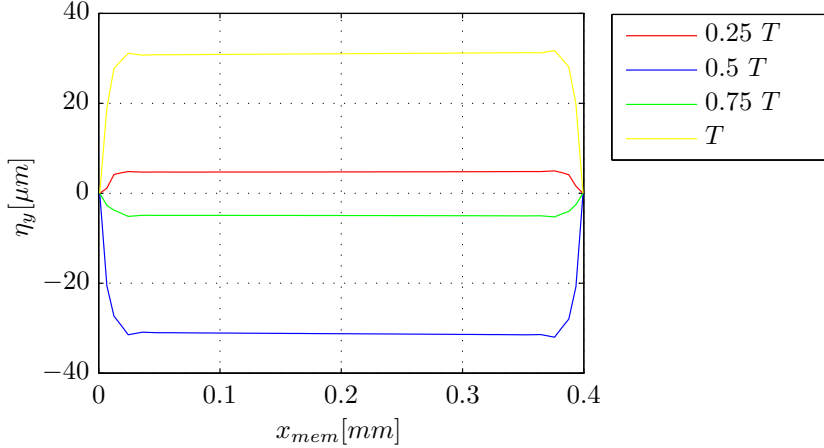


Figure 4.39: Displacements along y -direction of mph membrane at four different timesteps.

displacements along x produce only strain of the membrane, but does not input a signal the microphone. On the contrary the displacements along the y direction produce an effective signal that is processed by the microphone. The signal gathered by the mph on a period, and after the simulation reaches regime, is presented in fig. 4.40; the pressure values are computed in dB .

As it can be noticed from the figure, the signal reaches around $13 dB$ during its period; this value is reasonable large and can be easily perceived by the intracochlear receiver. As a result, also from the point of view of the microphone the configuration seems feasible at $1 kHz$. A complete study on the matter should include a study on all the range of frequencies on which a cochlear implant works; for this reason the present study cannot be considered complete, further simulations must be run and further improvements must be implemented. Nevertheless, this preliminary work provided useful new information and has paved the way for further investigations.

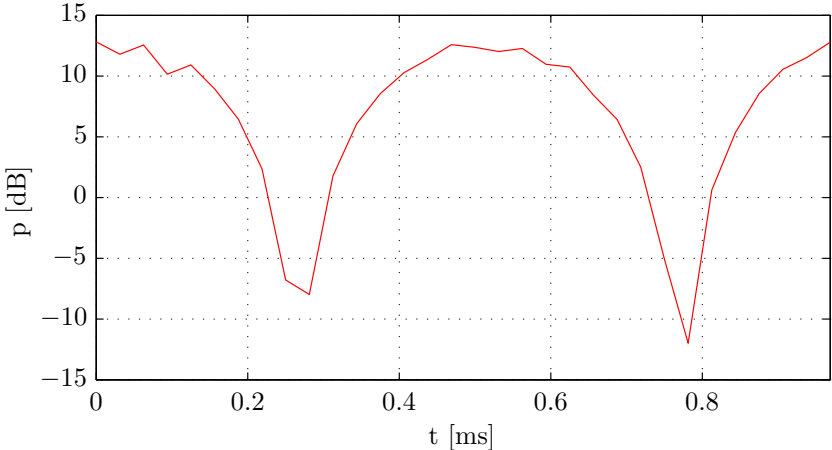


Figure 4.40: Pressure signal gathered by the microphone within a period of oscillation of the OW

Chapter 5

Conclusions

Now that the work has been explained and the main steps and results have been shown, it is time to draw some conclusions. This thesis can be basically divided into two parts, which will be discussed separately.

In the first part, the traditional box for cochlear simulation has been modified to simulate the pressure field more accurately in the region of the Round Window. The main characteristics of the proposed cochlear box were inspected and, afterwards, a comparison with experimental results was made. The results coming out from these simulations were satisfactory; the proposed arrangement of the box displays better agreement with experimental results. Besides, there are some favorable properties of this new box which agree better with physical expectations.

As a consequence, this new box was chosen to implement the microphone model. This part has to be considered only a first approach to the problem of numerical simulation of intracochlear receivers. This first study provides however important information on where to place the microphone inside the cochlea; furthermore it gives some broad information on the feasibility of this new kind of cochlear implants, which seems to work at the tested frequency.

For the future, further improvements of the code are necessary. In particular, the model of the microphone walls should be refined, as the walls

in the current model allow a velocity that is non-zero on their surfaces. The values for the stiffness of the membrane should be chosen following experimental results (see [18] for example). In addition it is necessary to carry out a study on the whole frequency range over which these devices should work.

Acknowledgements

The first person that I would like to thank is prof. Bottaro, for he gave me the possibility to do this work at ETH Zurich. Besides I would like to thank him for his availability and his support, and for the great courses he teaches which inspired me to choose the matter of this thesis.

A special thank goes also to Dominik Obrist; his weekly support, his ideas and his availability allowed all the results that I achieved in this study. I am also grateful for his patience, characteristics that was necessary to deal with me during this six months project.

I would like to thank my family, Mamma, Papà, Andrea, Ale, Augusto and the little mouses Boss and Lady. There are no words to express all the things I would like to tell them, and I am grateful for that. I'm thankful to Andri, we have grown up and in the same time stayed child together, I think there are no enough words also for this. I am grateful to my fellow students Zac and Giorgione, without them these 5 years of university wouldn't have been so easy and for some aspects so enjoyable. Finally I would like to thank Voja and Sedat, you gave me more than I could have ever expected in these six months, and together with them all the friends for having been here in these 5 years.

References

- [1] D. Kasper, A. Fauci, S. Hauser, D. Longo, J. Loscalzo, J. Jameson, *Harrison's principles of internal medicine*, McGraw-Hill, 18th edition, 2011.
- [2] D. Obrist, *Fluid mechanics of the inner ear*, habilitation treatise in Fluid Mechanics at ETH Zurich, 2011.
- [3] R. Nobili, F. Mammano, J. Ashmore, *How well do we understand the cochlea?*, Trends in Neurosciences, 21, pp. 159-167, 1998.
- [4] D. Obrist, *Cochlear Mechanics*, Lecture Notes for Bio-fluid-dynamics, ETH Zurich, 2013.
- [5] E. Edom, D. Obrist, L. Kleiser, *Simulation of fluid flow and basilar membrane motion in a two dimensional box model of the cochlea*, AIP Conference Proceedings, 1403, pp. 608-610, 2011.
- [6] R. Henniger, *Direct and large-eddy simulation of particle transport processes in estuarine environments*, dissertation ETH Zurich no. 19656, 2011.
- [7] C.S. Peskin, *Numerical analysis of blood flow in the earth*, J. Comput. Phys., 25, pp. 220-252, 1977.
- [8] E. P. Newren, A. L. Fogelson, R. D. Guy, R. M. Kirby, *A comparison of implicit solvers for the immersed boundary equations*, Comput. Methods Appl. Mech. Engrg., 197, pp. 2290-2304, 2008.

References

- [9] E. Givelberg, J. Bunn, *A comprehensive three-dimensional model of the cochlea*, J. Comput. Phys., 191, pp. 377–391, 2003.
- [10] A.J. Hudspeth, *Making an effort to listen: mechanical amplification in the ear*, Cell Press, Neuron 59, pp. 530-545, 2008.
- [11] S. Camalet, T. Duke, F. Jülicher, J. Prost, *Auditory sensitivity provided by self-tuned critical oscillations of hair cells*, PNAS, 97, pp. 3183-3188, 2000.
- [12] R. P. Beyer, *A computational model of the cochlea using the immersed boundary method*, J. Comput. Phys., 98, pp.145–162, 1992.
- [13] R. Verzicco, P. Orlandi, *A finite-difference scheme for three-dimensional incompressible flows in cylindrical coordinates*, J. Comput. Phys., 123, pp.402–414, 1995.
- [14] A. Moctezuma, J. Tu, *An overview of cochlear implant systems*, lectures notes for BIOE 414, University of Illinois, 2011.
- [15] E. A. Fadlun, R. Verzicco, P. Orlandi, J. Mohd-Yusof, *Combined immersed-boundary finite-difference methods for three-dimensional complex flow simulations*, J. Comput. Phys., 161, pp.35-60, 2000.
- [16] J. H. Sim, M. Chatzimichalis, M. Lauxmann, C. Rösli, A. Eiber, A. M. Huber, *Complex stapes motions in human ears*, JARO, 11, pp. 329–341, 2010.
- [17] H. H. Nakajima, W. Dong, E. S. Olson, S. N. Merchant, M. E. Ravics, John J. Rosowski, *Differential intracochlear sound pressure measurements in normal human temporal bones*, JARO, 10, pp. 23–36, 2008.
- [18] L. Prochazka, *Development of an intracochlear acoustic receiver for fully implantable cochlear implants*, extended feasibility study of ETH, 2013.
- [19] NIDCD, *Cochlear implants*, NIH Publication No. 11-4798, 2011.

References

- [20] M. B. Lesser, D. A. Berkley, *Fluid mechanics of the cochlea*, J. Fluid Mech., 51, part 3, pp. 497-512, 1972.
- [21] J. Lighthill, *Acoustic streaming in the ear itself*, J. Fluid Mech., 239, pp.551-606, 1992.
- [22] D. Goldstein, R. Handler, L. Sirovich, *Modelling a no-slip flow boundary with an external force field*, J. Comput. Phys., 105, pp. 354-366, 1993.
- [23] D. Manoussaki, E.K. Dimitriadis, R.S. Chadwick, *Cochlea's graded curvature effect on low frequency waves*, Phys. Rev. Lett., 96, 2006.

List of Figures

2.1	Anatomy of human ear [4].	4
2.2	Anatomy (left) and physiology (right) of human ear [14].	5
2.3	Coiled human cochlea [2].	6
2.4	Cross section of the cochlea [4].	7
2.5	Organ of Corti [2].	8
2.6	Schematic of a travelling wave provoked by a sinusoidal oscillation of the stapes [3].	9
2.7	Tonotopic map of frequency decomposition [4].	9
2.8	Ear with a cochlear implant [19].	11
2.9	Intracochlear receiver [14].	12
2.10	Example of immersed boundary curve (Γ), in a fluid domain (Ω) and described by the function $\mathbf{X}(\mathbf{s}, \mathbf{t})$	14
3.1	2-D box for cochlear simulation	19
3.2	Schematic of the interactions between the components and processes of the cochlea (OHC is the acronym for outer hair cells)[2].	20
3.3	Flowchart of the solution procedure.	22
3.4	Box features common to all the simulations	24
3.5	Non-dimensional velocity of the oval window plotted as a function of non-dimensional time.	25
3.6	Staggered grid in two dimension next to the boundaries, where: $x_1 \equiv x$, $x_2 \equiv y$, $u_1 \equiv u$ and $u_2 \equiv v$	28

List of Figures

3.7	Box arrangement of base configuration.	33
3.8	Portion of the grid implemented for the base configuration.	34
3.9	Cochlea layout ("RW" stands for round window, "Stap" for stapes)[17].	35
3.10	Box configuration with moved RW.	36
3.11	Membrane shape resulting from eq. 3.19 with a 1 : 1 aspect ratio of the axes.	37
3.12	Case 2, distance of 0.75 mm between the RW and the corner.	38
3.13	Case 3, distance of 1.5 mm between the RW and the corner.	38
3.14	Illustration showing the locations of various types of recordings carried out by Nakajima: pressure in scala vestibuli (P_{SV}), pressure in scala tympani (P_{ST}), pressure in the ear canal (P_{EC}), velocity of the stapes (V_{Stap}), velocity of the round window (V_{RW}) [17].	41
3.15	The means and standard deviations of the pressures in scala vestibuli and scala tympani relative to the ear canal pressure [17].	43
3.16	Mean magnitude of the translation velocity at the footplate center ($ v _{OZ}$), and its maximum possible errors $ v_{OZ} _{MPE}$ [16].	43
3.17	Procedure followed for the comparison with experimental result, "IFD ETH" is the numerical code implemented in this work.	44
3.18	Photograph of left temporal bone showing pressure sensors inserted into scala vestibuli (P_{SV}) and scala tympani (P_{ST}).	46
3.19	Measurement points ('x' markers in cyan) in the first box configuration tested.	46
3.20	Measurement points ('x' markers in cyan) in the second box configuration tested.	47
3.21	Box configuration with the hole next to the RW.	48
3.22	Cochlear box with mph model (cyan and blue lines).	49
3.23	Portion of the cochlear box with mph model (cyan and blue lines).	50

List of Figures

3.24	Distribution of the wall forces on the fluid grid with the new δ defined: \circ indicates the Eulerian grid, \bullet the Lagrangian one.	52
4.1	Instantaneous BM motion along y with BC at four different timesteps, $f = 1kHz$	57
4.2	Instantaneous BM motion along y with MRW at four different timesteps, $f = 1kHz$	58
4.3	Instantaneous BM motion along n with PC1 at four different timesteps, $f = 1kHz$	58
4.4	Instantaneous BM motion along the y -direction with BC at four different timesteps, $f = 4kHz$	59
4.5	Instantaneous BM motion along the y -direction with MRW at four different timesteps, $f = 4kHz$	60
4.6	Instantaneous BM motion along n with PC1 at four different timesteps, $f = 4kHz$	60
4.7	Envelope of BM displacements along the y -direction with BC at the three frequencies tested.	62
4.8	Envelope of BM displacements along y with MRW at the three frequencies tested.	63
4.9	Envelope of BM displacements along n with PC1 at the three frequencies tested.	63
4.10	CP displacement for each configuration and frequency tested.	64
4.11	Mean over a period of the velocity magnitude ($ \bar{u} $) in the BC at $1 kHz$	65
4.12	Mean over a period of the velocity magnitude ($ \bar{u} $) in the MRW at $1 kHz$	66
4.13	Mean over a period of the velocity magnitude ($ \bar{u} $) in the PC1 at $1 kHz$	66
4.14	Vector plot and velocity magnitude field of a sector of the cochlea at $t = 0.25T$ with PC1, the white dots indicate BM's points.	67

List of Figures

4.15	Vector plot and velocity magnitude field of a sector of the cochlea at $t = 0.5T$ with PC1, the white dots indicate BM's points.	67
4.16	Vector plot and velocity magnitude field of a sector of the cochlea at $t = 0.75T$ with PC1, the white dots indicate BM's points.	68
4.17	Vector plot and velocity magnitude field of a sector of the cochlea at $t = T$ with PC1, the white dots indicate BM's points.	68
4.18	Mean over a period of the velocity magnitude ($ \bar{u} $) in the MRW at 4 kHz.	69
4.19	Mean over a period of the velocity magnitude ($ \bar{u} $) in the PC3 at 1 kHz.	70
4.20	Maximum pressure oscillation field in the BC at 1 kHz. . .	71
4.21	Maximum pressure oscillation field in the MRW at 1 kHz. .	72
4.22	Maximum pressure oscillation field in the PC1 at 1 kHz. .	72
4.23	Maximum pressure oscillation field in the PC3 at 1 kHz. .	72
4.24	Maximum pressure oscillation field and measurement points with MRW at 1 kHz.	74
4.25	Maximum pressure oscillation field and measurement points with MRW in the vicinity of the RW at 1 kHz.	75
4.26	Comparison of MRW results with experimental data, which lie in the dashed blue lines whereas the solid blue line indicates their mean value.	76
4.27	Maximum pressure oscillation field and measurement points with PC1 at 1 kHz.	77
4.28	Maximum pressure oscillation field and measurement points with PC1 in the vicinity of the RW at 1 kHz.	77
4.29	Comparison of PC1 results with experimental data, which lie in the dashed blue lines whereas the solid blue line indicates their mean value.	78
4.30	Instantaneous BM motion along n with PC1 at four different timesteps, $f = 1kHz$	80

List of Figures

4.31	Instantaneous BM motion along n with MPH at four different timesteps, $f = 1kHz$	80
4.32	Envelope of BM's displacements along n for PC1 and MPH.	81
4.33	Mean over a period of the velocity magnitude ($ \bar{u} $) in the PC1 at 1 kHz	82
4.34	Mean over a period of the velocity magnitude ($ \bar{u} $) in the MPH at 1 kHz	82
4.35	Sector next to the microphone model of the mean over a period of the velocity magnitude ($ \bar{u} $) in the MPH at 1 kHz	83
4.36	Maximum pressure oscillation field in the PC1 at 1 kHz	83
4.37	Maximum pressure oscillation field in the MPH at 1 kHz	84
4.38	Displacements along the x -direction of the mph membrane at four different timesteps.	85
4.39	Displacements along y -direction of mph membrane at four different timesteps.	86
4.40	Pressure signal gathered by the microphone within a period of oscillation of the OW	87

Contents

Abstract	v
Prefazione	vii
1 Introduction	1
2 Literature review	3
2.1 Hearing process	3
2.1.1 The auditory system	4
2.1.2 Anatomy of the cochlea	5
2.1.3 Physiology of the Cochlea	8
2.2 Cochlear implant	10
2.3 Immersed boundary method	13
3 Method	17
3.1 Computational model of the cochlea	17
3.1.1 Hypotheses of the model	17
3.1.2 Insight into the hypotheses	18
3.2 Solution procedure	21
3.2.1 Simulation parameters	23
3.2.2 Solver for fluid flow equations	26
3.2.3 Computation of external forces on the fluid	30
3.3 Constant OW's velocity simulations	31
3.3.1 Base configuration	33

Contents

3.3.2	Problems of the base configuration	34
3.3.3	Configuration with moved RW	35
3.3.4	Proposed configuration	36
3.4	Comparison with experimental results	41
3.4.1	Results of Nakajima et al. [17]	41
3.4.2	Results of Sim et al. [16]	42
3.4.3	Procedure for the comparison	44
3.5	Configuration with the microphone	47
3.5.1	Cochlear box with the hole	47
4	Results	55
4.1	Constant OW's velocity simulations	56
4.1.1	BM's displacement	56
4.1.2	Velocity field	65
4.1.3	Pressure field	70
4.2	Comparison with experimental data	73
4.2.1	Comparison with the results from the MRW	74
4.2.2	Comparison with the results from the PC	75
4.3	Implementation of the microphone	79
4.3.1	BM's displacement	79
4.3.2	Velocity field	81
4.3.3	Pressure field	83
4.3.4	Dynamic of mph's membrane	84
5	Conclusions	89
	Acknowledgements	91

